Application of thermal ion-molecule reactions in tackling spectroscopic inferences in inductively coupled plasma mass spectrometry

By

Yong Wang

A thesis presented to the Department of Chemistry

in partial fulfillment of the requirements

for the degree of Master of Science

Brock University

St. Catharines, Ontario

August, 2011

Abstract

Part I: Ultra-trace determination of vanadium in lake sediments: a performance comparison using O_2, N_2O, and NH_3 as reaction gases in ICP-DRC-MS

Thermal ion-molecule reactions, targeting removal of specific spectroscopic interference problems, have become a powerful tool for method development in quadrupole based inductively coupled plasma mass spectrometry (ICP-MS) applications. A study was conducted to develop an accurate method for the determination of vanadium in lake sediment samples by ICP-MS, coupled with a dynamic reaction cell (DRC), using two different chemical resolution strategies: a) direct removal of interfering ClO^+ and b) vanadium oxidation to VO^+. The performance of three reaction gases that are suitable for handling vanadium interference in the dynamic reaction cell was systematically studied and evaluated: ammonia for ClO^+ removal and oxygen and nitrous oxide for oxidation. Although it was able to produce comparable results for vanadium to those using oxygen and nitrous oxide, NH_3 did not completely eliminate a matrix effect, caused by the presence of chloride, and required large scale dilutions (and a concomitant increase in variance) when the sample and/or the digestion medium contained large amounts of chloride. Among the three candidate reaction gases at their optimized conditions, creation of VO^+ with oxygen gas delivered the best analyte sensitivity and the lowest detection limit (2.7 ng L^{-1}). Vanadium results obtained from fourteen lake sediment samples and a certified reference material (CRM031-040-1), using two different analyte/interference separation strategies, suggested that the vanadium mono-oxidation offers advantageous performance over the conventional method using NH_3 for ultra-trace vanadium determination by ICP-DRC-MS and can be readily employed in relevant environmental chemistry applications that deal with ultra-trace contaminants.

Part II: Validation of a modified oxidation approach for the quantification of total arsenic and selenium in complex environmental matrices

Spectroscopic interference problems of arsenic and selenium in ICP-MS practices were investigated in detail. Preliminary literature review suggested that oxygen could serve as an effective candidate reaction gas for analysis of the two elements in dynamic reaction cell coupled ICP-MS. An accurate method was developed for the determination of As and Se in complex environmental samples, based on a series of modifications on an oxidation approach for As and Se previously reported. Rhodium was used as internal standard in this study to help minimize non-spectral interferences such as instrumental drift. Using an oxygen gas flow slightly higher than 0.5 mL min^{-1}, arsenic is converted to $^{75}As^{16}O^{+}$ ion in an efficient manner whereas a potentially interfering ion, $^{91}Zr^{+}$, is completely removed. Instead of using the most abundant Se isotope, ^{80}Se, selenium was determined by a second most abundant isotope, ^{78}Se, in the form of $^{78}Se^{16}O$. Upon careful selection of oxygen gas flow rate and optimization of RPq value, previous isobaric threats caused by Zr and Mo were reduced to background levels whereas another potential atomic isobar, $^{96}Ru^{+}$, became completely harmless to the new selenium analyte. The new method underwent a strict validation procedure where the recovery of a suitable certified reference material was examined and the obtained sample data were compared with those produced by a credible external laboratory who analyzed the same set of samples using a standardized HG-ICP-AES method. The validation results were satisfactory. The resultant limits of detection for arsenic and selenium were 5 ng L^{-1} and 60 ng L^{-1}, respectively.

Acknowledgement

I am indebted to a number of people and organizations that were integral to the completion of this thesis. Foremost, I would like to express my gratitude to my supervisor, Dr. Ian Brindle, for offering me this precious opportunity to pursue a master degree at Brock University. The course of this two-year study under his guidance was truly a lifetime experience that was filled with inspiring lessons, eye-opening ideas, and encouraging conversations. Thank you for making my academic journey such an enjoyable, educational, and rewarding one.

I would also like to thank Mr. Ernest Quan, a senior product specialist at PerkinElmer Canada and more importantly, a close friend of mine, for the immeasurable support and friendship that he offered me along the way. This thesis would not have been possible without his ever available help.

Thank you to my supervisory committee members, Dr. Heather Gordon and Dr. Tomas Hudlicky, for their direction and advice. The author also wants to thank members of Brock chemistry department for their support and friendship.

I gratefully appreciate the research funding provided by Brock University and Ontario Ministry of Environment throughout. PerkinElmer Canada is thanked for the training course sponsored. I also thank Mrs. Paula Cheese and Niagara Regional Laboratory for their cooperation in two successful research projects.

I dedicate this thesis to my family, especially my wife, Lynn, for their eternal trust, support, and love.

Table of Contents

List of Tables

List of Figures

Chapter 1: Introduction

1.1 Spectroscopic interferences in ICP-MS

The past couple of decades have witnessed a rapid growth of the use of inductively coupled plasma mass spectrometry instrumentations (ICP-MS) in the area of analytical atomic spectroscopy, thanks to its unrivaled performance characteristics, such as detection power, multi-element capability, and analytical speed, to name but three. Along the way, the history of ICP-MS can also be regarded as a long-term battle against spectroscopic interferences in that those 'uninvited guests' in mass spectra have remained a significant challenge to the quality of ICP-MS analysis. The definition or characterization of a spectroscopic interference in ICP-MS is fairly straightforward. In the commonest sense, any ionic species with the same mass to charge ratio (m/z) as the analyte ion of interest is deemed a spectroscopic interference.[1] Depending on their compositional and ionic attributes, spectroscopic interferences are routinely divided into three categories:[2] isobaric (atomic) interferences, polyatomic (molecular) interferences, and doubly charged interferences.

1.1.1 Isobaric (atomic) overlaps

This type of interference refers strictly to the spectral overlap between analyte of interest and isotope(s) of neighbouring elements that have nominally the same mass-to-charge ratio, for instance, ^{40}Ar on ^{40}Ca, ^{64}Ni on ^{64}Zn, and ^{74}Se on ^{74}Ge. Because most naturally occurring elements from the periodic table have more than one isotope with varying isotopic abundances[a],

[a] See Appendix I for a comprehensive list of isotopic abundances.

analysts are often able to chose a suitable isotope that is free from isobaric interferences to avoid spectral overlaps (with the only exception of indium,[3] whose both isotopes are interfered with other elemental isotopes). Mathematical correction is frequently used to cope with such inter-element overlaps, if the interfering element happens to have another isotope that does not exhibit spectral interference.[4]

1.1.2 Polyatomic (molecular) interferences

The formation of polyatomic ions, also known as molecular or adduct ions, poses perhaps the most complex interference problem in ICP-MS applications and can undermine the accuracy of analytical data for a number of elements. As their name suggests, these ions consist of at least two atomic species (e.g. $^{40}Ar^{16}O^+$ on $^{56}Fe^+$, $^{35}Cl^{16}O^+$ on $^{51}V^+$, and $^{40}Ar^{35}Cl^+$ on $^{75}As^+$) and remain stable during their passage through the quadrupole mass analyzer. Reference 1 provides a thorough summary of commonly encountered polyatomic interferences, which are routinely observed, in fairly high abundances, in the forms of hydride, argide, oxide, chloride, and sulfide in ICP-MS practice. The mechanisms of creation of such interferences are multifaceted, mainly due to (a) ion-molecule interactions between major species in the plasma, that occur during the ion extraction or expansion processes,[5] (b) recombination reactions occurring near the 'boundary layer' formed around the edge of aperture of the sampling cone,[6] and (c) incomplete dissociation of refractory oxide species in the plasma as a result of strong bond strength.[7] The extent of a potentially significant polyatomic interference can also be very case specific, largely depending on the analyte chosen for determination, sample composition, as well as the digestion matrix. In the early stage of ICP-MS practice, severe polyatomic interference problems were often dealt by sophisticated sample treatment procedures (sample dissolution,[8] precipitation,[9] solvent

extraction,[10] on-line separation,[11] etc.), or alternative sample introduction methods, including laser ablation,[12] hydride generation,[13] and desolvation,[14,15] to avoid introducing molecular-ion-prone oxygen, chlorine and sulfur.[16] Cold plasma methods[17] were popular for a while for the purpose of attenuating argon-and-chlorine related molecular ions in ICP-MS applications, since a lower voltage used for ICP RF (radio frequency) power would have an immediate effect on the reduction of undesired precursor ions, such as Ar^+, O^+, Cl^+, owing to their high ionization potentials. Nevertheless, despite the efforts made on the suppression of polyatomic ions, these measures were either vulnerable to contamination, caused by additional sample handling steps, or were only applicable for determination of special sample types and a limited number of elements.

1.1.3 Doubly charged ions

Compared with most ions formed in plasma that are singly charged, doubly charged ions are relatively rare, as only few elements' second ionization energy (typically alkaline earth metals and light rare earth elements) is lower than the first ionization energy of argon (15.8 eV).[18] The impacts of doubly charged ions can be effectively minimized by optimization of the ICP-MS system, in particular the ICP RF power and nebulizer gas flow rate, which keeps the occurrence of doubly charged ions at a level that is insignificant relative to their co-residing analyte ions.

1.2 Current ICP-MS instrumentations

Amongst a handful of mass analyzers developed since the inception of ICP-MS to the analytical market, the radiofrequency quadrupole mass analyzer has gained the most popularity over its competitors and has thus far become the primary technique retained by the majority of analytical

laboratories for metal determination, owing to its outstanding analytical performance and moderate cost.[19] However, acknowledging the fact that, at the current stage of ICP-MS technology, formation of various polyatomic interferences seems inevitable, one conspicuous limitation typical in quadrupole-based ICP-MS is that, it is largely unable to separate two overlapping ions because the RF-driven quadrupole commonly operats at a low resolution of 0.7-1.0 amu.[20]

In order to tackle the interference problems without significantly altering the instrumental design and complicating the laboratory operation, tremendous research efforts were then made on the development of an 'analyte pre-filter', inspired by the successful application of tandem quadrupole MS/MS systems in organic mass spectrometry, and ultimately led to remarkable technological breakthroughs and commercial successes that have resulted in the current 'state-of-the-art' collision/reaction cell technologies.[21,22,23] By exploiting different types of ion-molecule interactions, the introduction of the collision/reaction cell to conventional quadrupole ICP-MS allows immediate *in-situ* reduction of the intensity of interfering species in post-plasma ion beams by orders of magnitude. The working principles and fundamental differences between these two approaches were described in a comprehensive review by Tanner *et al.*[24] In short, the extracted ion beam is first guided into a gas-pressurized cell prior to entering the quadrupole mass analyzer to undergo a series of ion-molecule interactions. Collision cell (ICP-CC-MS) instruments, which employ light and non-reactive gases, such as hydrogen, helium, or mixtures of the two, use non-thermal ion-molecule collision and subsequent kinetic energy discrimination (KED)[25,26,27] techniques to achieve analyte/interference separation. Reaction cell (RC) based instruments, which utilize heavier and more reactive gases, such as ammonia, oxygen, and methane, selectively promote primary ion-molecule reactions under near thermal

conditions.[28,29,30] Recognizing that newly launched ICP-MS instruments with different cell technologies exhibit comparable analyte transmission and detection capability, Tanner *et al.* (ref 24) pointed out that, in many cases, the utilization of specific thermal ion-molecule reactions in RC could facilitate resolving polyatomic interference entrained in post-plasma ion beam, thanks to selectivity and efficiency of those reactions. By introducing an appropriate reaction gas, which is intended to boost thermal bimolecular ion-molecule reactions with either the interfering polyatomic ions or the analyte ions, and optimizing the reaction gas flow rate, as well as the low-mass rejection parameter, RPq (also known as the dynamic bandpass tuning parameter)[b], of the cell quadrupole, 'chemical resolution' of the specific interference problem can be realized. This unique 'tandem' quadrupole arrangement and other important functioning units of the DRC[c] (dynamic reaction cell) are portrayed in Figure 1.

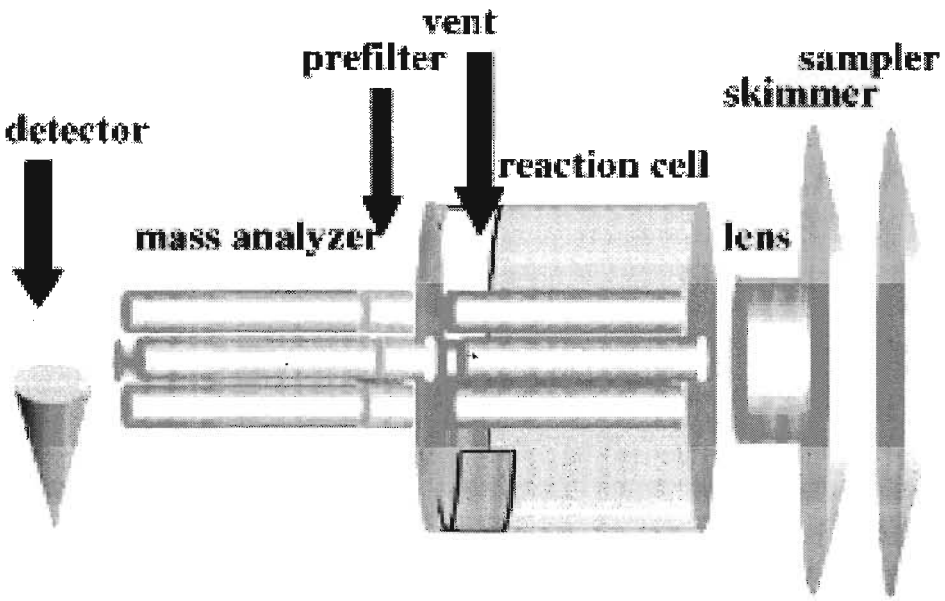

Figure 1: 3D schematic diagram of the DRC.[31]

[b] The use of term 'RPq' is thoroughly described in ref. 24.
[c] The DRC is a proprietary technology of PerkinElmer Inc., USA.

1.3 Guiding principles of thermal ion-molecule chemistry based method development in ICP-MS practices

Our laboratory is equipped with a dynamic reaction cell inductively coupled plasma mass spectrometer (ICP-DRC-MS), so making proper use of thermal ion-molecule chemistry is central to successful method development, aiming to address relevant spectroscopic interference problems. One advantageous feature of a reaction cell based ICP-MS over its collision cell counterpart is that, the method development component that deals with spectral overlaps can be very versatile. Because the gas choice and the analyte ion selection using reaction cell technology are no longer restricted to the criteria that are applied rigorously to collision cell ICP-MS, they can be conveniently adjusted as circumstances arise. Inspired by the pioneering research on thermal ion-molecule interactions in ICP-MS by Douglas and Tanner's groups,[22,24] Hattendorf and Günther[32] and Olesik and Jones[33] elaborated this approach in a detailed strategy for method development regarding spectral interference removal in quadrupole reaction cell ICP-MS, taking advantage of the well-established database of thermal ion-molecule chemistry[34,35,36]. In their opinion, careful selection of a reaction gas is always the first, and probably the most decisive step that supports a sound method to tackle specific interferences in ICP-MS.

To be a candidate reaction gas for resolving a particular spectral interference problem, the thermodynamic profile of the proposed ion-molecule reaction needs to have the following characteristics: 1) The intended reaction must be exothermic ($\Delta H_{rxn} = \sum \Delta H_f(\text{products}) - \sum \Delta H_f(\text{reactants}) < 0$) so that it can take place at the near-thermal temperature regime in the reaction cell; 2) The reaction gas reacts with only one of the overlapping ions (or one reaction markedly outpaces the other, if reactions with both analyte and interference ions occur simultaneously) ; 3) The kinetic rate constant of the reaction must be large enough to generate a detectable analyte

signal that is stable over the (very short) period of instrumental analysis. In practice, the analytical performance of a DRC based ICP-MS method depends largely on how well these prerequisites are satisfied.

Once a reactive gas is chosen and an analyte ion to be measured is defined in the proposed method (whether in its atomic form or in an artificially created polyatomic form), a thorough investigation on potential spectral interferences in regard to the defined analyte ion (the resultant ion formed after reaction with the cell gas) should be carried out so as to ensure no new significant threats to the accuracy of measuring the analyte ion emerge. This step comprises reaction cell conditioning and system optimization and aims to purify the analyte signal and maximize the signal-to-background ratio for the analyte ion. The effectiveness and robustness of the proposed method will eventually be subject to a validation procedure where analytical figures of merit, such as linear dynamic range, limit of detection, accuracy, as well as precision, for suitable certified reference material(s) in complex matrices, are rigorously evaluated.

Part I: Ultra-trace determination of vanadium in lake sediments: a performance comparison using O_2, N_2O, and NH_3 as reaction gases in ICP-DRC-MS[37]

Chapter 2: Overview of determination of V^+ in ICP-MS

In the research described in the first half of this thesis the focus was on removal of the $^{35}Cl^{16}O^+$ interference from which elemental analysis of vanadium by conventional ICP-MS suffers. Vanadium, whose predominant isotope, $^{51}V^+$, has an abundance of 99.75%, is often compromised by the presence of this polyatomic ion since ICP-MS analysis essentially demands that the ^{51}V isotope be used for determination. The severity of the vanadium (Figure 2) interference problem is especially evident from a number of environmental and clinical studies[38,39] that involve trace or ultra-trace determination of vanadium where samples require either concentrated HCl, as part of the digestion medium that uses *aqua regia*, or have high salinity, such as sea water, urine, and serum. Where vanadium is present in high chloride matrices, interference with the $^{51}V^+$ analyte signal is inevitable and the accuracy of the determination will diminish unless the analyst resorts to more expensive high resolutions ICP-MS, where a typical resolution of 2500-3000[40,41] is necessary to separate two isobars.[d]

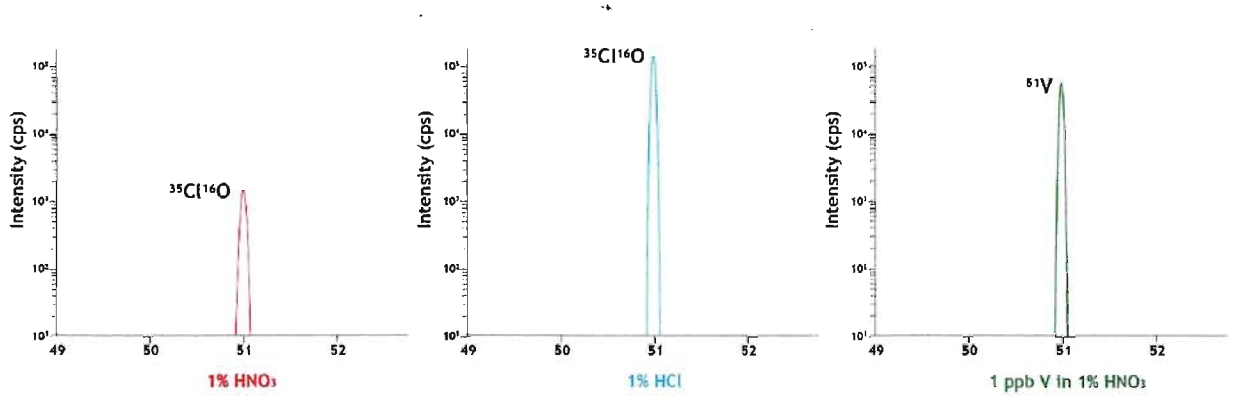

Figure 2: The severity of ClO^+ interference in various matrices.

[d] R=m/Δm. The atomic (molecular) masses of the two isobars: ^{51}V (50.94396), $^{35}Cl^{16}O$ (50.96377).

In order to liberate $^{51}V^+$ ion from the abundant polyatomic interference, $^{35}Cl^{16}O^+$, traditionally NH_3 has been recommended to react with ClO^+ through a charge transfer route (reaction 1) without significantly affecting the V^+ analyte:[33]

$$ClO^+ + NH_3 \rightarrow ClO + NH_3^+ \qquad k = 6.0\times10^{-10}\,cm^3s^{-1} \qquad (1)$$

This reaction is exothermic and proceeds at a fairly fast rate in the DRC. To date, ammonia has served as the reaction gas for vanadium determination for a wide variety of sample types[42,43,44,45,46,47] owing to its straightforward measurement and high efficiency of ClO^+ ion elimination. However, this method is not flawless as far as the accuracy of $^{51}V^+$ signal is concerned. Clemmer *et al.*[48] reported that vanadium actually suffers minor signal loss through a slow reaction with ammonia to form VNH^+ species ($k=2.2\times10^{-12}\,cm^3s^{-1}$). Olesik and coworkers[49] observed minor branching reactions between V^+ and NH_3forming $V(NH_3)_n^+$ species. The review by Tanner *et al.*[24] also mentioned that, at low RPq, a new interfering ion, NH_2Cl^+, at m/z 51, is very likely to occur, owing to an exothermic reaction between Cl^+ and NH_3 ($\Delta H_{rxn} = -25$ kcal/mol). Despite their slow reaction rates, the new interferences formed due to the use of ammonia inevitably result in increased uncertainty and complexity of the m/z 51 signal. Olesik confirmed that, at high gas flow rate or low RPq, ammonia becomes less effective at generating satisfactory signal-to-noise ratio for $^{51}V^+$ than at optimal DRC settings. In addition, the extent and implication of such matrix effects with this approach have received little attention in previous applications. In this context, seeking a different reaction gas, able to overcome the interference problem for vanadium with comparable or better analytical performance, would be a useful addition to the current ICP-MS method archive.

Aside from the conventional approach that removes ClO^+ species directly from the post-plasma ion beam, reaction of V^+ with another element/molecule to form a stable vanadium-containing ion provides a way around the ClO^+ interference issue. Bohme's group used various reactive gases[50,51,52,53,54] to explore the ion-molecule chemistry for a range of transition-metal ions. In the case of vanadium, it was found that oxygen (O_2, reaction 2) and nitrous oxide (N_2O, reaction 3) react rapidly with V^+ to give the primary reaction product VO^+, which has a nominal molecular mass of 67, by the following reaction pathways:

$$V^+ + O_2 \rightarrow VO^+ + O \qquad k=2.8\times10^{-10}\ cm^3s^{-1} \qquad (2)$$

$$V^+ + N_2O \rightarrow VO^+ + N_2 \qquad k=2.4\times10^{-10}\ cm^3s^{-1} \qquad (3)$$

The reaction rate constants for each reaction were experimentally determined with the state-of-the-art ICP-SIFT-MS (selected-ion flow tube) technique. On the other hand, the reactivity of interfering ClO^+ ion with oxygen and nitrous oxide had been ambiguous in the past. Koyanagi *et al.*[55] initially reported that ClO^+ is essentially unreactive towards both O_2 and N_2O under thermal conditions. Bandura *et al.*[56] later demonstrated that ClO^+ and N_2O do react to form a measurable ClO_2^+ background (reaction 4) when the chloride level in the matrix is high. At m/z 67 there also resides a minor Zn isotope (^{67}Zn, at 4.1% abundance). However, this mass could still be a candidate for V determination if the contribution from ClO_2^+ is insignificant, because ^{67}Zn is only very slightly interfered with by other polyatomic species and can be mathematically corrected by choosing an appropriate Zn isotope as a reference.[57]

$$ClO^+ + N_2O \rightarrow ClO_2^+ + N_2 \qquad (4)^e$$

$$VO^+ + N_2O \rightarrow VO_2^+ + N_2 \qquad k=5.2\times10^{-11}\ cm^3s^{-1} \qquad (5)$$

[e] Reported in ref 56, but no thermodynamic and kinetic information was mentioned.

Investigations of vanadium oxidation chemistry with O_2 and N_2O and their implications for vanadium determination were conducted by Tanner's and Bohme's groups. Under thermal conditions, VO^+ can not be further oxidized to VO_2^+ by oxygen, but nitrous oxide does react with VO^+ at a much slower rate to form VO_2^+ (reaction 5). Tanner's group (Bandura *et al.*[56]) reported that monitoring VO_2^+ ion (m/z 83) might be a possible solution for plasma-based vanadium determination, since isobaric interference is no longer a concern at m/z 83. They also reported that VO_2^+ afforded a better background equivalent concentration than VO^+, where a matrix consisting of 10 mg L^{-1} (ppm) V and 3.3% HCl was used. At the optimal point of their experimentation, the VO_2^+ signal was about 2 orders of magnitude higher than the background. At these higher levels of vanadium and chloride, both elevated analyte sensitivity of VO_2^+ at m/z 83 and concomitant increased background of ClO_2^+ at m/z 67 can be expected, resulting in improved signal-to-noise ratio at m/z 83 and reduced signal-to-noise ratio at m/z 67. However, if vanadium and chloride were determined at the much lower levels found in real-world applications, for instance at μg L^{-1}-equivalent levels, VO_2^+ would likely become unfavoured due to its significantly reduced signal-to-noise ratio.

Nitric oxide (NO) was reported to undergo similar vanadium oxidation steps as nitrous oxide, but the rate of yielding primary product VO^+ was unsatisfactory[36]. In addition, the simultaneous secondary reaction between the two primary products, VO^+ and N_2O, would further scatter the already-low V analyte. Therefore, the effectiveness of nitric oxide gas for efficient vanadium mono-oxidation appears questionable.

Other non-oxidative gases, such as monofluromethane (CH_3F) and carbon disulfide (CS_2) were also considered because of their modest reactivity towards V^+, but the idea was soon discarded due to inadequate reaction speed and creation of new difficult spectral overlaps. The primary

product of V^+ and CH_3F, $^{51}V^{19}F^+$, coincides with two other elemental isobars: ^{70}Ge (21.23% abundance) and ^{70}Zn (0.6% abundance). The reaction rate constant between V^+ and CS_2 (7.0×10^{-11} cm^3s^{-1}) is about one order of magnitude lower than that of oxygen and nitrous oxide, suggesting that the resultant V analyte may suffer a marked reduction in sensitivity. Its primary product, an adduct ion, $V^+\cdot(CS_2)$, also unfortunately overlaps with ^{127}I, the only isotope of iodine in nature. Therefore, we conclude that amongst those common reactive gases that are commercially available, only oxygen and nitrous oxide seem to be qualified to serve as alternative reaction gases to solve vanadium interference problems in ICP-MS. The key kinetic reaction rates of respective ion-molecule reaction are summarized in Table 1.

Table 1: Kinetic profile of selected V^+ ion-molecule reactions[36]

Candidate reaction gas	Products	k_{exp} (cm^3s^{-1})	Higher order products
O_2	$VO^+ + O$	2.8×10^{-10}	VO_3^+, VO_5^+, VO_7^+
NO+NO[f]	$VO^+ + N_2O$	2.1×10^{-11}	VO_2^+, NO^+
N_2O	$VO^+ + N_2$	2.4×10^{-10}	$VO_2^+(N_2O)_{0-3}$
CS_2	$V^+(CS_2)$	7.0×10^{-11}	$V^+(CS_2)_{2-3}$
CH_3F	VF^+	1.7×10^{-10}	$VF^+(CH_3F)_{1-5}$

K_{exp}: experimentally determined effective bimolecular rate coefficient

Environmental samples were considered appropriate for this study because they offer a good case for ultra-trace determination of vanadium where the ClO^+ interference problems appear to be likely. Recently, growing interest in vanadium's presence in the environment necessitates ultra-trace determination in various environmental samples. For instance, elevated concentrations of vanadium in sediments have been linked to oil pollution of natural water systems, since it is

[f] The corresponding kinetic data refers to the rate-determining step.

found in relatively high concentrations in crude oil and petroleum products.[58,59] To date, the determination of vanadium for environmental samples using an oxidation approach has been little reported and no comparative research with different reaction gases has yet been conducted. Therefore, a series of experiments was developed in the current study to test the proposed vanadium oxidation approach using oxygen and nitrous oxide for real-world environmental samples and to evaluate this approach with respect to the conventional method that uses NH_3.

Chapter 3: Experimental

3.1 Instrumentation

A PerkinElmer-SCIEX (Concord, ON, Canada) ELAN® DRC® II ICP-MS instrument was used for analyzing all samples and standards. The sample introduction system consists of a Meinhard® A3 type concentric nebulizer, a quartz baffled cyclonic spray chamber and a 2.0 mm (I.D.) quartz injector. The instrument was optimized on a daily basis to ensure that the baseline elemental sensitivities[g] recommended by the manufacturer were obtained. Peristaltic tubing was replaced every two days of use (roughly a total of 8-10 hours) to ensure performance consistency. Other important operating parameters of the instrument are listed in Table 2.

Table 2. Instrumental settings for ICP-DRC-MS (V analysis)

Plasma RF power (W)	1100
Plasma gas flow (L min^{-1})	15.0
Auxiliary gas flow (L min^{-1})	1.2
Nebulizer gas flow (L min^{-1})	0.86-0.88 (optimized daily)
Cell gas flow (mL min^{-1})	0.2-0.45 (optimized individually for NH_3, O_2 and N_2O)
RPa	0 for all analytes
RPq	0.45 (V-NH_3), 0.40 (V-O_2), 0.35 (V-N_2O)
Sample uptake (mL min^{-1})	~1.0
Interface	Pt sampler and skimmer cones
Auto lens calibration	On (Be 6.5V, Co 7.5V, In 8.5V. Slope = 0.01887, intercept = 6.35)
Analog Stage Voltage (V)	-1950
Pulse Stage Voltage (V)	1050
Cell Rod Offset Std (V)	-10.00
Discriminator Threshold (mV)	70.00
Cell Path Voltage Std (V)	-15.00
Axial Field Voltage (V)	250.00
Detector	Dual (optimized daily)
Scanning mode	Peak hopping
Dwell time (ms)	100
Sweeps	3
Replicate	3

[g] $^{24}Mg^{+}$ (1ng mL^{-1})>8000 cps, $^{115}In^{+}$ (1ng mL^{-1})>40000 cps, $^{238}U^{+}$(1ng mL^{-1})>30000 cps, Ba^{2+} /Ba^{+}(10ng mL^{-1})<3%, CeO^{+}/Ce^{+}(1ng mL^{-1})<3%.

3.2 Reagents[h]

Analytical-grade (single distilled) nitric acid (68-70% m/v) and hydrochloric acid (20-22% m/v) were purchased from Caledon (Georgetown, ON, Canada). Vanadium and Zinc stock solutions were purchased from High-Purity Standards (Charleston, SC, USA). All sample and working solutions were prepared with ultra-pure de-ionized water (18.2MΩ resistivity) from Elgastat-Maxima purification system (High Wycombe, UK). Certified reference material (CRM031-040-1)[i] was acquired from RTC (Laramie, WY, USA). Research grade ammonia (99.999%), argon (99.998%), nitrous oxide (99.998%), and oxygen (99.999%) gases were supplied by Praxair (Hamilton, ON, Canada).

3.3 Sample collection and preparation

Fourteen lake sediment samples were collected from various locations in the Niagara Region of Southern Ontario, including one duplicate, and were processed in the Niagara Regional Laboratory. Approximately 0.5 g of each sample and the standard reference material was digested by a standard *aqua regia* leach , employing a 3:1(v/v) HCl and HNO_3 mixture (15 mL and 5 mL, respectively). All samples had undergone 4 h of continuous heating at 95.0±5.0 °C. The resultant solutions were further treated with 7-8 mLs of hydrogen peroxide, and were heated for another 10 minutes. When cooled, ultra-pure DI water was added to form a 50 mL solution. In order to minimize the memory effects and to reduce the total digested solids concentration of the solution entering nebulizer capillary, all digestates were immediately diluted 1:100 (500 µL to 50 mL) with 0.5% (m/v) nitric acid for analysis. Good laboratory practices were faithfully undertaken to ensure that the analytical procedures were essentially free from random contamination.

[h] Manufacturing information of the reagents is listed in Appendix II.
[i] For verification of trace metal determination in sludge/sediment samples.

3.4 Calibration

Initially a background scan to determine vanadium intensity was performed for all diluted sample solutions with the purpose of selecting appropriate concentrations of vanadium calibration standards. Although the ICP-MS is designed to deliver a linear dynamic range over nine orders of magnitude in DRC mode, a narrower calibration range, which closely brackets intensities from all samples, would be preferred. A blank and five vanadium standards were then prepared at 0.5, 1.0, 5.0, 10.0, 20.0 $\mu g\ L^{-1}$ with 0.5% (m/v) nitric acid according to the information provided by the background V tests. Effort for matrix matching was made by spiking 50 µL HCl in each 50ml working solutions. At a later point in this study, a separate set of calibration standards was used (50, 100, 500, 1000, 2000 $ng\ L^{-1}$) to verify the data obtained from 1:5000 sample solutions. All vanadium calibration curves were linear through zero (blank subtracted) and delivered correlation coefficients of at least 0.9999[j].

3.5 Quality control of the analysis

Quality control was performed throughout the standardization and sample analysis procedures by means of careful instrument maintenance, repeated analyte signal calibration and verification with QC material. Sample introduction system was periodically maintained so as to prevent nebulizer clogging and chemical residual build-up in the spray chamber and injector tube. Internal standardization approach was not employed in the current study because two suitable elements recommended by the EPA method 6020, scandium (Sc) and yttrium (Y), tend to react with oxygen and nitrous oxide rapidly.[50,51] In order to monitor the instrument drift during the analysis, V analyte calibration was conducted every 30 minutes in combination with monitoring the indium signal from an independent indium standard solution (10 $ng\ mL^{-1}$). During the

[j] See Appendix III for details.

analysis, the recovery of QC material was also frequently compared with its certified value to ensure the current sample run was legitimate.

Chapter 4: Results and discussion

4.1 Selection of vanadium analyte ion

When ammonia is used as the reaction gas in the DRC, it is incontrovertible that ^{51}V would be the only meaningful m/z peak for vanadium analysis because the reaction between ammonia and V^+ is insignificant. The reactivity of V^+ towards oxygen was thoroughly examined by Koyanagi *et al.*,[60] when the reaction rate constants of a minor primary product VO_2^+ (reaction 6) and a major secondary product VO_3^+ (reaction 7) were found to be 300- and 1400-fold lower than that of VO^+ reaction (reaction 2). Such large differences in reaction rate constants make VO^+ the best ion for V determination.

$$V^+ + O_2 \rightarrow VO_2^+ \qquad k = 8.4\times10^{-12}\ cm^3s^{-1} \qquad (6)$$

$$VO^+ + O_2 \rightarrow VO_3^+ \qquad k = 2.0\times10^{-13}\ cm^3s^{-1} \qquad (7)$$

When nitrous oxide was used, however, in order to make a choice between VO^+ and VO_2^+, an experiment similar to that mentioned in Bandura *et al.*[56] was conducted. A modified solution, containing 10 μg L^{-1} (ppb) vanadium with HCl concentration in the matrix adjusted from 3.3% to 0.1%, which simulates the chloride level in prepared working solutions and diluted samples, was run with the RPq value set at 0.4. The reaction profiles of m/z 51, 67, and 83 at various N_2O flow rates are illustrated in Figure 2. It can be seen that, unlike the surprisingly low signal to background ratio for VO_2^+ observed from the optimization curves, the VO^+ analyte signal was about 2 orders of magnitude higher than the background, indicating that, at ultra-trace level, the VO^+ ion is appropriate to be used for vanadium determination for its superior sensitivity when N_2O serves as a reaction gas.

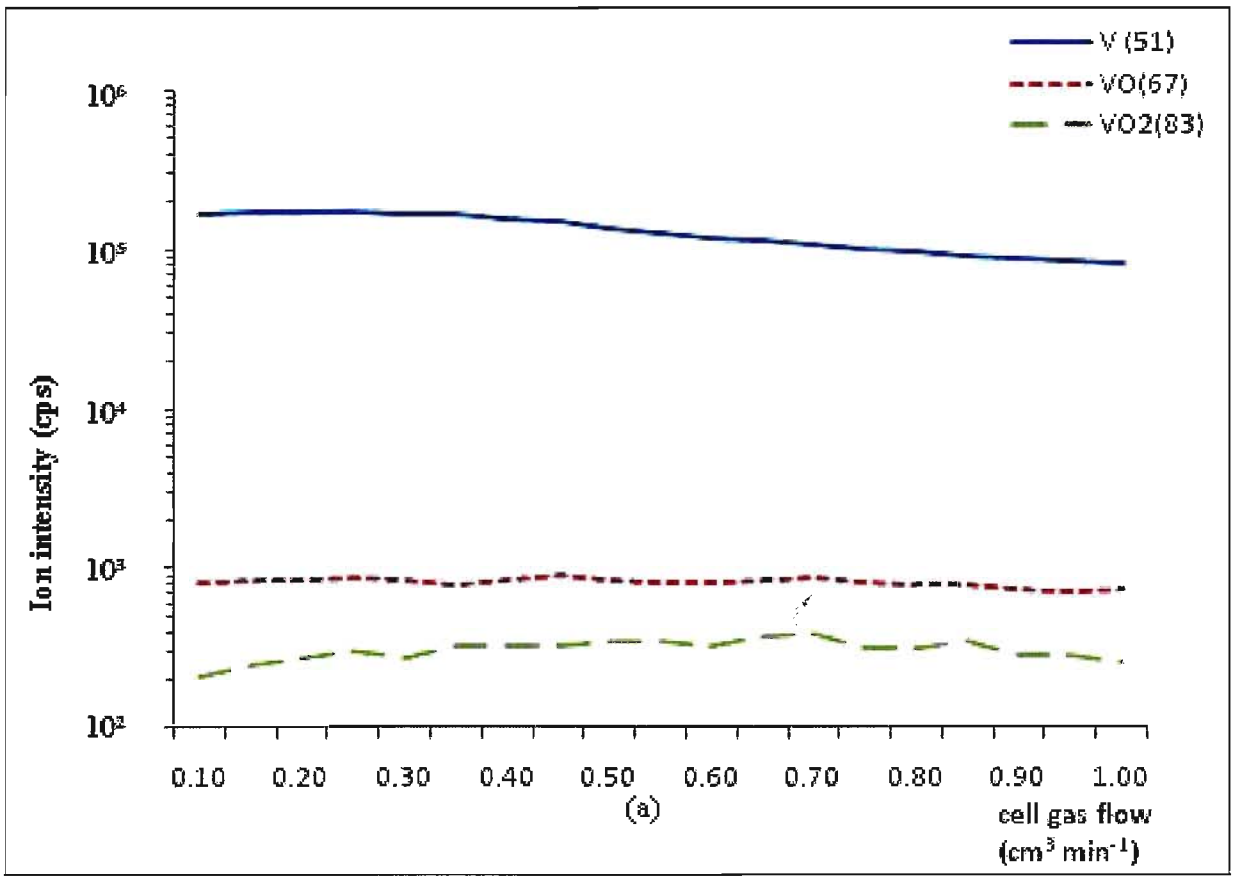

Figure 3. (a). Ion abundances (m/z 51, 67, 83) produced from a solution containing 0.1% HCl.

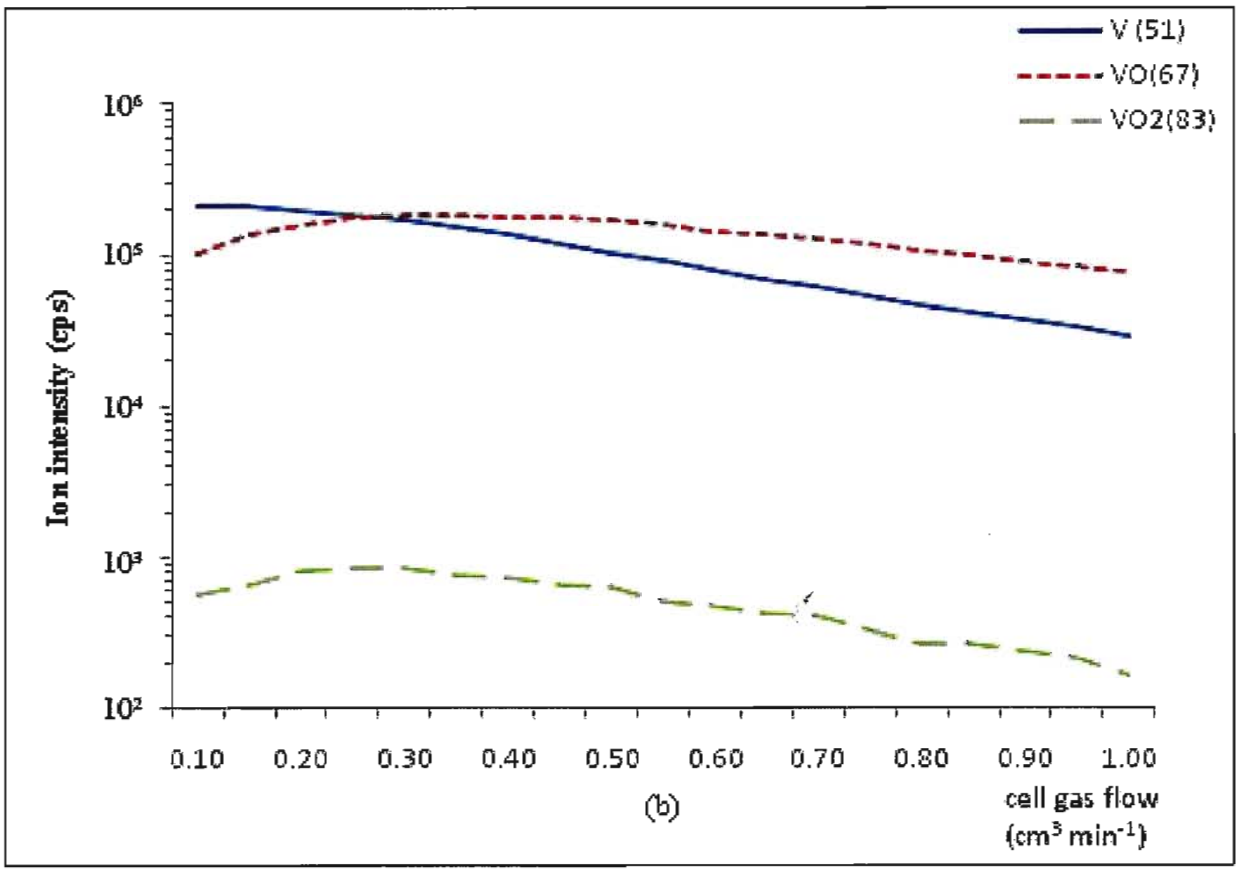

Figure 3. (b). Ion abundance (m/z 51, 67, 83) produced from a solution containing 10 µg L^{-1} V in 0.1% HCl matrix.

4.2 Cell gas flow and RPq optimization

Once the reaction gas choices have been confirmed, the optimization of DRC parameters becomes crucial in finding the best compromise between analyte ion intensity and the limit of detection for each reaction gas. To approximate the chloride concentration in diluted samples and working standards, 50µl of HCl was spiked into the optimization blank and 1µg L^{-1} V standard solutions (50ml final volume, 0.5% HNO_3 matrix). The effects of both cell gas flow rate and RPq values on ion intensity and the corresponding limit of detection are illustrated in Figures 3 and 4. With ammonia gas, the V^+ signal displayed a sharp decline when the gas flow increased from

0.5-0.8 cm^3 min^{-1} due to the occurrence of complex clustering reactions forming $V(NH)_m(NH_3)_n^+$ in this range[36, 61] and collisional scattering. The RPq test for ammonia indicated that 0.75 was the optimal value at which the lowest detection limit was achieved. In this range NH_2Cl^+ ion can also be substantially prevented because $^{35}Cl^+$ ion is largely eliminated by the cell quadrupole. However, a noticeable side-effect of such high RPq setting is a concomitant drop of V^+ analyte counts, in the current study, by 72%, from the peak maximum. Consequently, the RSDs of vanadium data will inevitably deteriorate due to the drastic reduction in analyte sensitivity. To compensate for such compromise in precision it is worthwhile to consider a lower RPq as long as the resultant detection limit is still reasonably low. In this regard, cell gas flow at 0.35 cm^3 min^{-1} and RPq at 0.45 were selected for use with the ammonia method. Oxygen and nitrous oxide gases for determinations of V^+ as VO^+ were optimized at cell gas flow rates of 0.35 and 0.25 cm^3 min^{-1}, respectively. Moderate RPq values (0.4 for oxygen and 0.35 for nitrous oxide) were used for measuring m/z 67 as the prevention of Cl^+, O^+, and S^+ from entering cell quadrupole becomes less important than maintaining the maximun V^+ analyte from the ion beam. It can be seen that the VO^+ signals exhibit smooth decay after the maxima were reached because of the slow secondary reactions taking place at increased in-cell gas density.

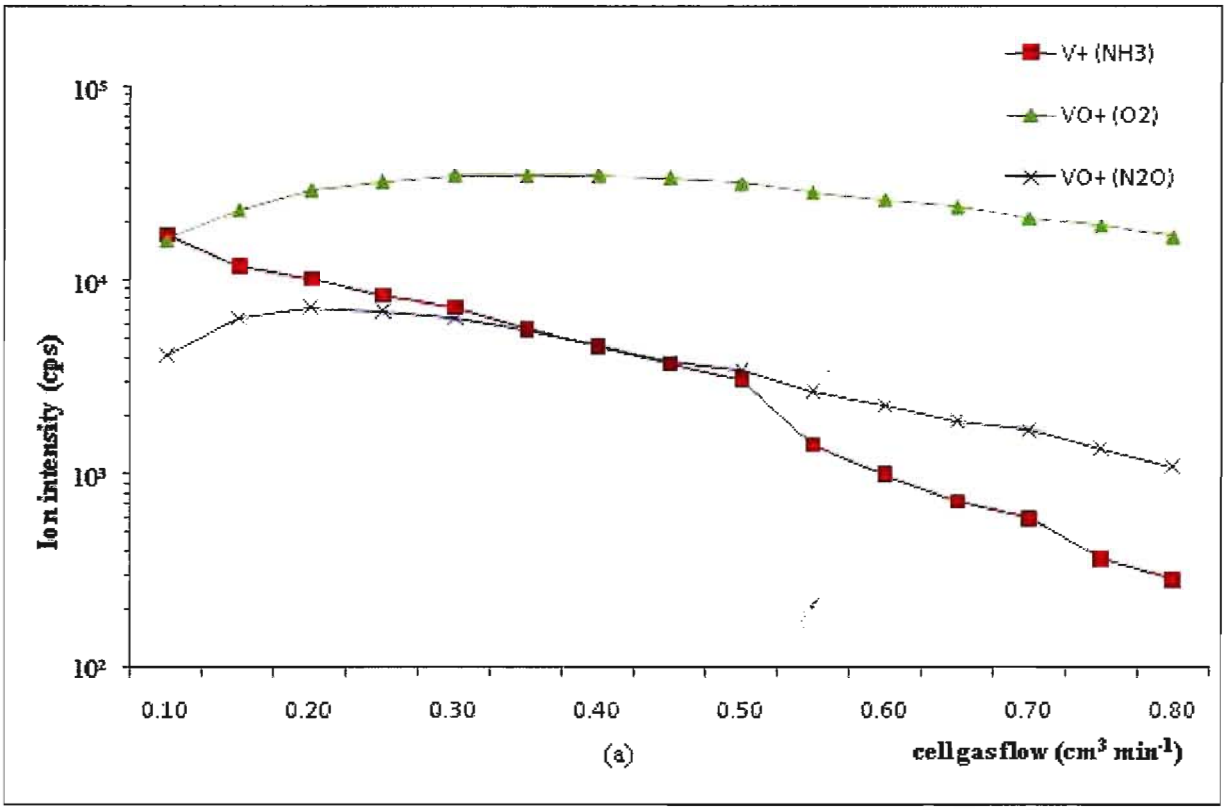

Figure 4 (a). Reaction gas flow rate optimization of DRC: analyte intensity as a function of cell gas flow rate.

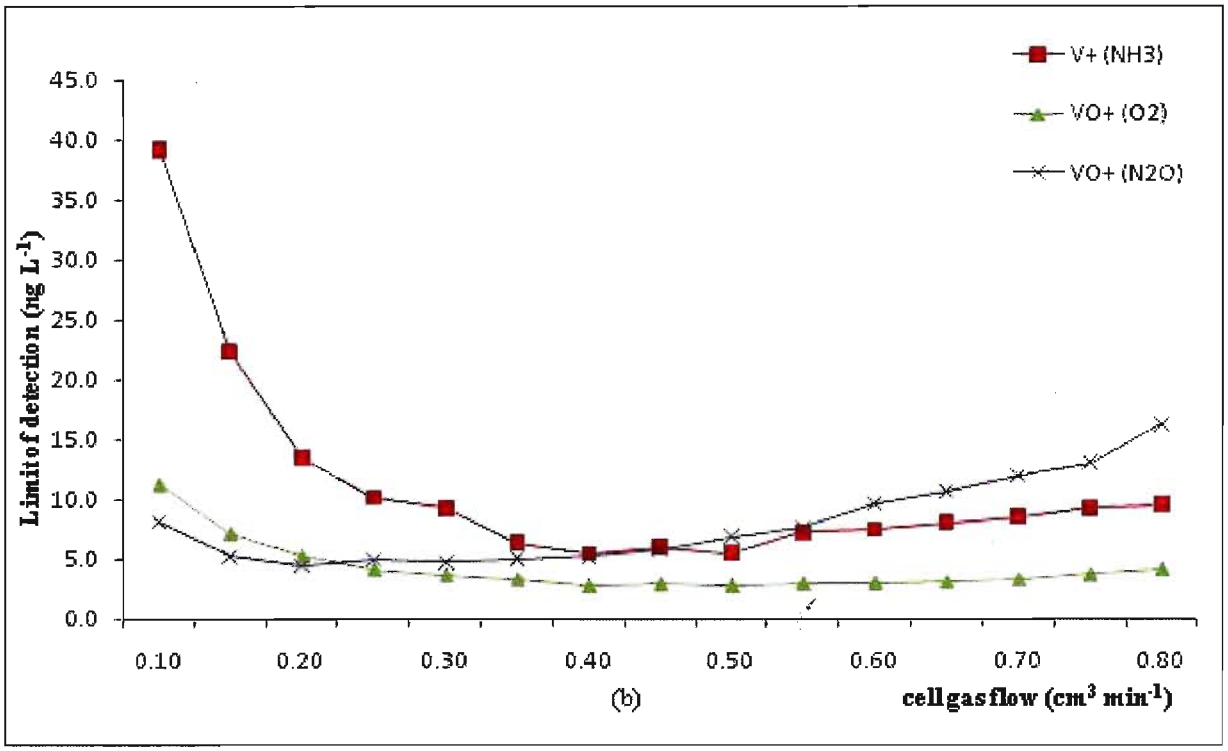

Figure 4 (b). Reaction gas flow rate optimization of DRC: limit of detection as a function of cell gas flow rate.

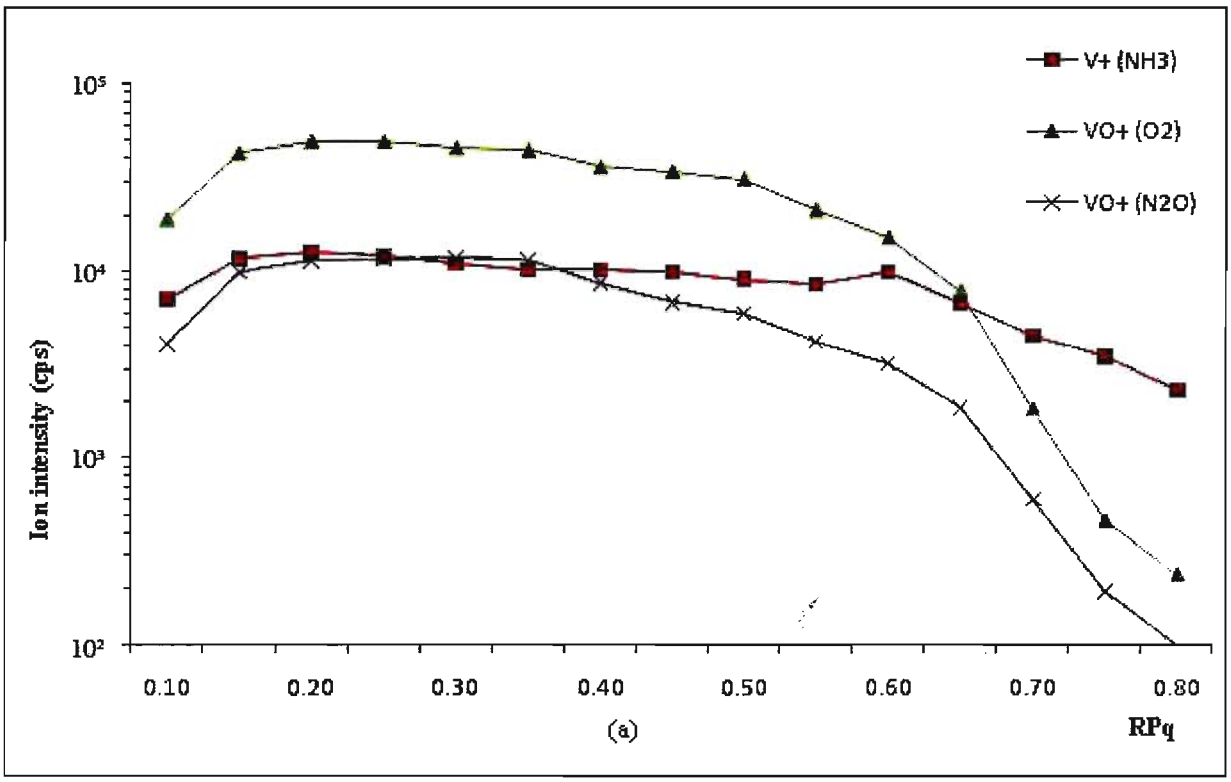

Figure 5 (a). RPq optimization of DRC: vanadium analyte intensity as a function of RPq

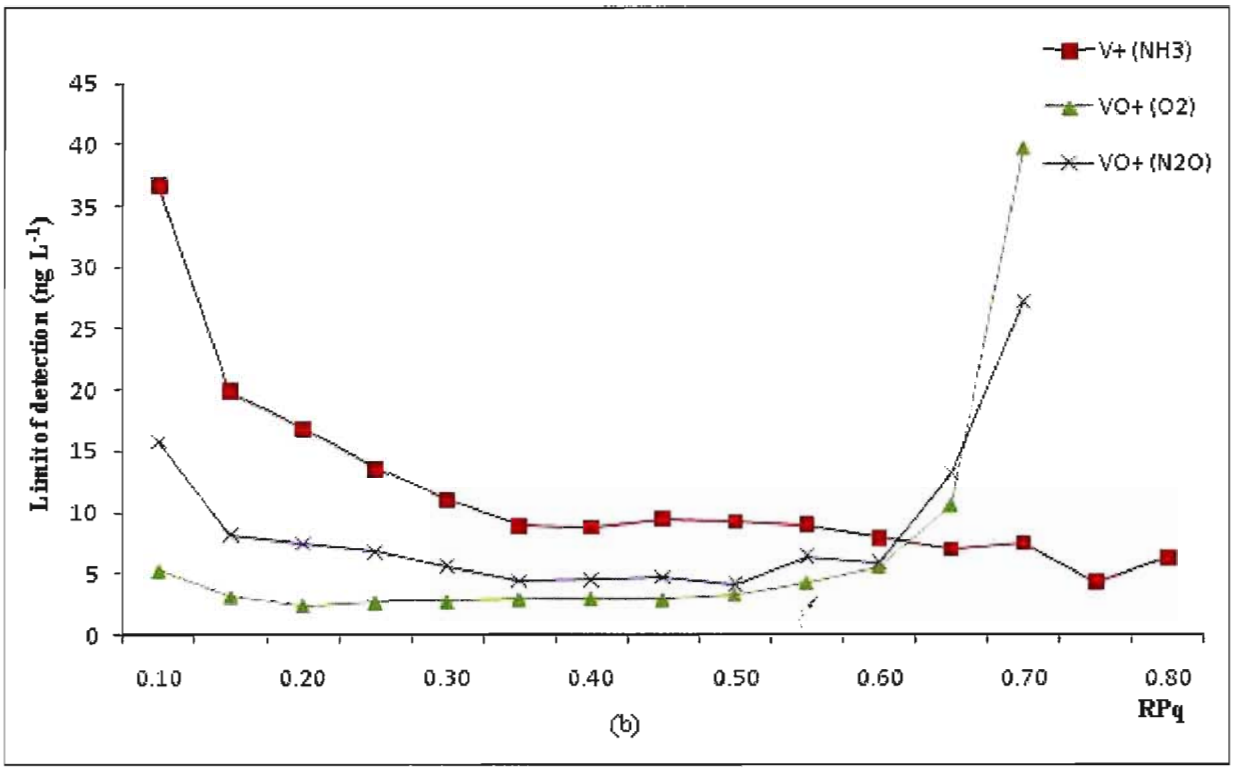

Figure 5 (b). RPq optimization of DRC: vanadium limit of detection as a function of RPq.

4.3 Zn correction for V^+ oxidation with O_2 and N_2O

The utilization of mathematical correction to restore the analyte signal from an interfered spectrum, where a simple, fast, and cost effective method is the aim of analysis, has a long history in ICP-MS applications.[62,63,64] However, it should be noted that such a theoretical approach is often subject to various practical complications and must be strictly verified before implementation. As mentioned earlier, although the proposed V^+ mono-oxidation can well protect the V analyte, the new analyte, $^{51}V^{16}O^+$ ion, ought to be corrected for the presence of $^{67}Zn^+$ and other co-residing polyatomic ions. Examples of potential spectral interferences for all zinc isotopes are listed in Table 3 as summarized by May and Wiedmeyer.[92]

Table 3. Interferences of Zinc isotopes in ICP-MS

Zn isotope (%)	Isobaric interferences (%)	Matrix-based polyatomic interferences	Plasma-based polyatomic interferences
^{64}Zn, (48.6)	^{64}Ni, (0.926)	$^{48}Ca^{16}O^+$, $^{48}Ti^{16}O$, $^{32}S^{16}O_2^+$, $^{32}S_2$, etc.	$^{36}Ar^{14}N_2^+$
^{66}Zn, (27.9)	-	$^{48}Ti^{18}O^+$, $^{34}S^{16}O_2^+$, $^{33}S_2$, $^{32}S^{17}O_2^+$, $^{32}S^{34}S$, etc.	-
^{67}Zn, (4.1)	-	$^{35}Cl^{16}O_2^+$, $^{34}S^{16}O^{17}O^+$, $^{33}S^{16}O^{18}O^+$, $^{33}S^{34}S^+$, $^{32}S^{16}O^{18}OH^+$, etc.	-
^{68}Zn, (18.8)	-	$^{52}Cr^{16}O^+$, $^{36}S^{16}O_2^+$, $^{34}S^{16}O^{18}O^+$, $^{33}S^{17}O^{18}O^+$, $^{34}S_2^+$, $^{35}Cl^{16}O^{17}O^+$, etc.	$^{40}Ar^{14}N_2^+$, $^{36}Ar^{32}S^+$
^{70}Zn, (0.6)	^{70}Ge, (21.23)	$^{35}Cl_2^+$, $^{35}Cl^{17}O^{18}O^+$, $^{37}Cl^{16}O^{17}O^+$, $^{36}S^{16}O^{18}O^+$, $^{36}S^{17}O_2^+$, etc.	$^{40}Ar^{14}N^{16}O^+$, $^{38}Ar^{32}S^+$, $^{36}Ar^{34}S^+$

Amongst all zinc isotopes, ^{64}Zn and ^{70}Zn are apparently unsuitable for correcting ^{67}Zn due to multiple sources of interferences. ^{66}Zn and ^{68}Zn suffer interferences mainly from polyatomic ions, but ^{66}Zn also overlaps with $^{48}Ti^{18}O^+$, which is the primary product of $^{48}Ti^+$ (73.8% abundance) and reaction gases (O_2 and N_2O). The formation of TiO^+ is exothermic and proceeds at a comparable reaction rate[45,46] as VO^+. Therefore, the utility of using ^{66}Zn to correct for the interference from ^{67}Zn is limited to non-titanium containing samples only.

$$Ti^+ + O_2 \rightarrow TiO^+ + O \qquad k = 4.6\times10^{-10}\ cm^3s^{-1} \qquad (8)$$

$$Ti^+ + N_2O \rightarrow TiO^+ + N_2 \qquad k = 5.3\times10^{-10}\ cm^3s^{-1} \qquad (9)$$

$^{52}Cr^{16}O^+$ ion was thought to be the interference of greatest concern for m/z 68 if an oxidation approach was used, relative to the abundance of Cr in samples. An early study by Armentrout *et al.*[65] revealed the endothermic nature of reactions of Cr^+ with O_2 and N_2O. Recent ICP-SIFT-MS experiments[45,46] suggested that $^{52}Cr^{16}O^+$ ion does not pose a threat to m/z 67 as the rates of

Cr^+ oxidation with O_2 (reaction 10) and N_2O (reaction 11) are extremely low. Other polyatomic interferences for m/z 68 are multifold, but with blank subtraction their impacts can be largely neutralized. The low background on this mass can also be related to (a) sulfur-related interferences were not formed in large quantity due to the low sulfur presence in those sediment samples , and (b) the slow formation reactions and poor in-cell stability of those tri- and tetra-atomic ions. If sulfur's concentration is high in samples, a higher low-mass cutoff value can be used to minimize the impact, though the sensitivity of VO^+ analyte might be slightly affected as well (Figure 5(a) provides an illustrative reference for proper selection of an RPq for VO^+).

$$Cr^+ + O_2 \rightarrow CrO_2^+ \qquad k = 2.2\times10^{-13}\ cm^3s^{-1} \qquad (10)$$

$$Cr^+ + N_2O \rightarrow CrO^+ + N_2 \qquad k = 1.5\times10^{-13}\ cm^3s^{-1} \qquad (11)$$

Hence, ^{68}Zn seems to be the only isotope that is capable of correcting for ^{67}Zn. A mathematical equation: $I(^{51}V^{16}O) = I(67) - \frac{A(67_{Zn})}{A(68_{Zn})} \times I(68) = I(67) - 0.218 \times I(68)$, was then applied for VO^+ signal correction. The validity of this equation was tested using 1 μg L^{-1} V standard with a 5 μg L^{-1} Zn spike in 0.5% (m/v) nitric acid, mimicking the ratio of V and Zn in the QC material. The recovery of vanadium was close to unity, suggesting that this correction equation is a workable approach for vanadium determination through oxidation in DRC.

4.4 Sample analysis

4.4.1 Accuracy, precision, and detection limit

Vanadium results from fourteen lake sediment samples and a certified reference material are listed in Table 4. The accuracy of the methods was evaluated with recovery rates from a certified reference material (CRM031-040-1) and a series of paired *t*-tests within the experimental data. All mean vanadium values and their associated relative standard deviations (RSDs) were obtained from eight consecutive measurements. Method detection limit was computed by the commonly accepted protocol that uses three times the standard deviation of calibration blank. Excellent vanadium recovery data suggested that the mathematical correction for Zn was very effective. Table 5 shows that with 1:100 dilution, results from ammonia approach differed significantly from those using oxidation approach, whereas results from oxygen and nitrous oxide oxidation showed no significant differences. At the cost of larger RSDs, the accuracy of vanadium data from using the ammonia approach was improved when a dilution of 1:5000 was utilized although, compared with the oxygen method, large standard deviations were generated as the dilution was so high to deal with the stubborn matrix effect. Calibration slopes from each method revealed that V/VO^+ analyte sensitivity increased in the sequence of ammonia, nitrous oxide and oxygen roughly by a factor of three. Oxygen gas also presented the best RSDs (0.21-0.99%) and limit of detection (2.7 ng L^{-1}), thanks to the stable and high yield of VO^+. In this study the use of nitrous oxide as DRC gas for ultra-trace vanadium determination was successfully proved by delivering moderate VO^+ sensitivity and comparable limit of detection with oxygen and ammonia methods. Initial expectations, based on the predicted rate of the reaction, suggested that nitrous oxide would produce sensitivity of VO^+ ion similar to that

delivered by oxygen. The comparatively low VO^+ yield was probably due to simultaneous secondary oxygen transfer and collisional losses, as N_2O is a much heavier gas than O_2. To examine sample preparation and other laboratory-specific errors, all in-house vanadium data were compared with data from the Niagara Regional Laboratory, who employed ICP-AES for the analysis of samples and used the same set of sample digestates. It can be seen from Table 4 that the accuracy of vanadium results was satisfactory.

Table 4. Analytical figures of merit for the vanadium determination methods

Sample ID	NH_3 (mg kg^{-1})[a]	NH_3(mg kg^{-1})[b]	O_2(mg kg^{-1})[a]	N_2O (mg kg^{-1})[a]	ICP-AES (mg kg^{-1})[c]
45939	$30.5_1\pm0.3_4$	$29.2_0\pm0.5_1$	$27.4_9\pm0.1_1$	$29.3_8\pm0.2_2$	28.36
45984	$24.3_0\pm0.2_6$	$20.4_7\pm0.3_2$	$19.8_1\pm0.1_3$	$20.2_3\pm0.2_6$	20.10
45991	$34.5_1\pm0.4_9$	$29.3_7\pm0.3_3$	$28.8_0\pm0.1_5$	$29.0_3\pm0.1_8$	28.92
45994	$25.8_8\pm0.1_6$	$24.8_1\pm0.7_8$	$24.3_2\pm0.1_4$	$25.1_4\pm0.1_6$	24.55
45994-2	$26.3_9\pm0.2_4$	$24.8_0\pm0.7_7$	$23.9_7\pm0.0_7$	$25.1_1\pm0.0_9$	24.40
46046	$36.3_2\pm0.2_5$	$32.6_9\pm0.6_4$	$31.3_2\pm0.1_2$	$32.7_8\pm0.3_0$	32.32
46051	$48.8_3\pm0.3_9$	$41.7_4\pm0.4_4$	$42.2_1\pm0.0_9$	$42.0_6\pm0.1_8$	42.05
46113	$25.8_5\pm0.1_7$	$24.2_2\pm0.6_0$	$23.6_5\pm0.1_2$	$23.5_2\pm0.2_0$	23.25
46114	$188.4_2\pm0.4_8$	$174.2_5\pm2.1_9$	$174.8_7\pm0.8_0$	$173.9_9\pm0.6_6$	173.00
46131	$12.6_4\pm0.1_2$	$12.2_9\pm0.4_1$	$11.5_5\pm0.1_1$	$11.7_6\pm0.1_8$	11.30
46145	$27.6_6\pm0.4_1$	$25.7_7\pm0.9_2$	$25.1_1\pm0.1_3$	$26.3_0\pm0.1_6$	25.95
46166	$40.9_5\pm0.3_4$	$41.5_1\pm1.0_7$	$41.5_1\pm0.1_1$	$41.4_3\pm0.3_0$	40.33
46167	$37.5_9\pm0.3_6$	$42.3_1\pm1.0_3$	$41.3_6\pm0.1_9$	$41.9_4\pm0.3_1$	41.17
46257	$18.5_8\pm0.3_1$	$18.4_2\pm0.3_5$	$17.9_5\pm0.1_3$	$18.4_2\pm0.2_1$	17.77
CRM031-040[d]	$311.5_7\pm1.6_9$	$297.0_9\pm2.8_9$	$297.6_7\pm1.6_5$	$301.8_9\pm1.8_9$	-
M.R. (%)[e]	105.06	100.18	100.37	101.80	-
RSDs (%)[f]	0.26-1.48	0.97-3.58	0.21-0.99	0.35-1.51	-
Calibration slope (cps per ng mL^{-1})	7677.6	7639.4	21178.7	10813.3	-
C.C.[g]	0.999996	0.999987	0.999997	0.999996	-
L.O.D. (ng L^{-1})[h]	3.3	3.1	2.7	8.7	-

a. 1:100 dilution of digestate b. 1:5000 dilution of digestate
c. Determined at wavelength of 292.402 nm as suggested in EPA method 6010C
d. Reference value of vanadium: 296.56±23.40 mg kg^{-1}, 277.97-315.14 mg kg^{-1} at 95% C.I.
e. Method recovery
f. n=8
g. Correlation coefficient
h. Calculated by 3σ of calibration blank/slope

Table 5: Paired *t*-tests for vanadium data

	NH_3 [a]/ O_2 [a]	NH_3 [a]/ N_2O [a]	O_2 [a] / N_2O [a]	NH_3 [b]/ O_2 [a]	NH_3 [b]/ N_2O [a]	NH_3 [a]/ NH_3 [b]
t(exp)[c]	3.18	2.68	0.20	2.84	0.65	2.54

a. 1:100 dilution of digestate; b. 1:5000 dilution of digestate; c. Two-tailed $t_{(0.05, 14)} = 2.14$

4.4.2 Matrix effect

Although matrix induced spectral interference problems in ICP-DRC-MS analysis are normally expected to be resolved readily with the aid of additive reaction gas and band-pass tuning capability, for ultra-trace elemental determination, they can still be observed if the method is not sufficiently robust. In this study it was quite evident with the ammonia approach since, when 1:100 diluted sample solutions were analyzed, the vanadium results obtained were consistently higher than with the vanadium oxidation approach by 3-16%. This elevation in values can largely be attributed to the mismatch of the matrices between samples and the calibration standards because the chemical constituents in the samples remain unknown to the analyst regardless of the matrix matching efforts made. In other words, if the chloride concentration differs considerably amongst sample solutions, it is virtually impossible to prepare a blank solution and calibration standards that are able to represent variable background concentrations of chlorine for all samples. In Figure 6 it can be seen that, at low ammonia flow rates, matrices containing varying amount of HCl produced significantly different background at m/z 51, suggesting incomplete removal of ClO^+ and NH_2Cl^+ for matrices containing high chloride concentrations. Although the ClO^+ background could be reduced to similar levels by increasing ammonia gas flow rates to 0.6-0.7 mL min^{-1}, these flow rates were far from optimum. The other approach to overcome the matrix-induced interference problem is to use a high RPq value (>0.65) to reduce the amount of chlorine from entering the DRC, thus preventing ClO^+ and NH_2Cl^+ ion from forming. However, this reduction of background is usually achieved at the

expense of significant loss of analyte sensitivity. In this study we report that, if moderately greater RSDs are deemed acceptable to the analysis, a higher dilution factor for the sample solutions may be considered to alleviate the matrix effect, by reducing the chloride concentration in samples to a level such that, at optimized cell gas flow, a near-uniform background of mass 51 be produced without excess vanadium signal loss. With the revised dilution factor and calibration standards, as previously mentioned, the data discrepancy between methods was significantly reduced and excellent linearity of the calibration curve was still obtained, thanks to reduced variation in analyte background in samples, as well as to strong detection capability of the DRC instrument at levels of tens to thousands of nano-grams per litre. In contrast to ClO^+ removal with ammonia gas, oxidation of V^+ is virtually unaffected by matrix composition and can be run at lower dilution factors to achieve better analyte sensitivity and precision.

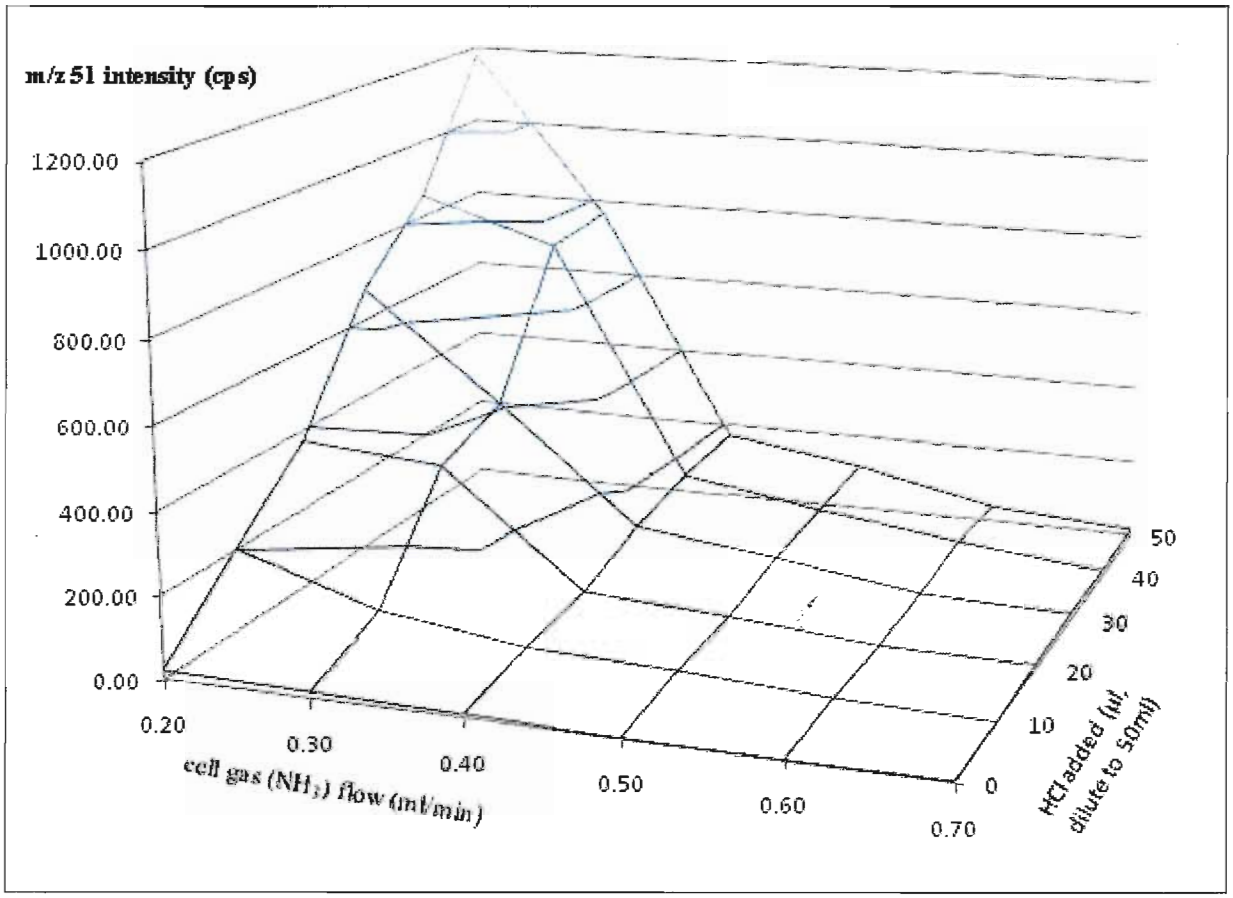

Figure 6. Effect of ammonia gas flow rate and presence of Cl on ClO^+ background.

Chapter 5: Conclusions and future prospects

Three reaction gases examined in this study, ammonia, oxygen, and nitrous oxide, demonstrate their practical feasibility for effective separation of vanadium analyte from its major polyatomic interference, $^{35}Cl^{16}O^{+}$, in environmental samples. Amongst the three reaction gases, oxygen generated the best sensitivity and the lowest detection limit for vanadium. Although the limits of detection obtained from the three methods were essentially identical, the ammonia approach exhibited considerable susceptibility to matrix chloride levels, whereas vanadium oxidation with oxygen and nitrous oxide was quite robust and showed no susceptibility to chloride at the suggested dilution factor. The selection of cell operating parameters and appropriate dilution factor for the samples appeared very important in balancing analyst's needs and analytical performance. With each method in optimized conditions, the vanadium data produced for fourteen lake sediment samples and a certified reference material agreed generally well with each other and were verified by an external laboratory. Last but not least, the oxidation of V^{+} with oxygen and nitrous oxide proved to be an effective V-determination strategy that can be readily employed in ultra-trace environmental applications.

At present, our research efforts are to validate this proposed V oxidation method in determination of other types of environmental samples, such as sludge and waster water. Future work is also considered mainly on verification of the effectiveness and robustness of this approach for more complex matrices, i.e. geological materials that requires tougher digestion media (HF and $HClO_4$ involved) and probably contain much higher chloride content, as well as biological samples that engage with organic matrices.

Part II: Validation of a modified oxidation approach for the quantification of total As and Se in complex environmental matrices

Chapter 6: Overview of determination of As and Se by ICP-MS

Arsenic and selenium are always high on the list of elements that necessitate environmental monitoring, primarily due to their well-known health hazards to humans and animals. The presence of these two toxic elements in the environment can mainly be ascribed to anthropogenic activities, such as mining operations, industrial discharges, and the erosion of geological forms naturally enriched with these elements.[66,67] Though ubiquitously distributed in the nature, the concentrations of As and Se observed are generally low (often at mg L^{-1} levels or lower) especially in aquatic environments (such as marine,[68,69] freshwater,[70] wastewater[71]) and soil for agricultural purposes,[72] where pollution monitoring mandates are legally enacted by various levels of governmental organizations[k]. In the case of Ontario, arsenic and selenium levels in the environment are rigorously regulated[73,74] to ensure drinking water and food safety. For instance, the maximum acceptable concentrations for arsenic and selenium in drinking water are 0.025 and 0.01 mg L^{-1}, respectively. Thus, the ability to accurately quantify these two elements at trace to ultra-trace level is of special importance in delineating the state of environmental pollution and requires techniques with extraordinarily powerful detection capabilities in this instance.

Before ICP-MS became a preferred technique for elemental analysis, a number of analytical methods had been developed for the determination of arsenic and selenium in various matrices. Hydride generation (HG) has been popular for As and Se quantification for its high selectivity and sensitivity and coupling with various detectors has been reported. Veber *et al.*[75] adopted a HG-AAS setup following a pre-concentration procedure of the two elements. Brindle's team[76,77]

[k] See Appendix IV for a partial list of relevant legislations and regulations.

interfaced HG with a DCP-AES system that afforded detection limits at low ng mL^{-1} levels. Schramel and Xu[78] used a more powerful HG-ICP-AES hyphenation which delivered comparable detection capability as Brindle's work. Direct determination with ETAAS was also reported.[79,80] Acknowledging the delicacy and success these techniques have presented, it is also noted that their performance is sometimes restricted to sophisticated instrumental hyphenation. Additional sample handling, such as speciation, pre-reduction, and pre-concentration are often required. Furthermore, the limited detection capability for As and Se of those techniques hinders determination at much lower levels, for instance, at ng mL^{-1} levels. Therefore, a simpler, faster, and more powerful technique for determination of As and Se, able to iron out the problems that have troubled the analysts previously, would be appreciated.

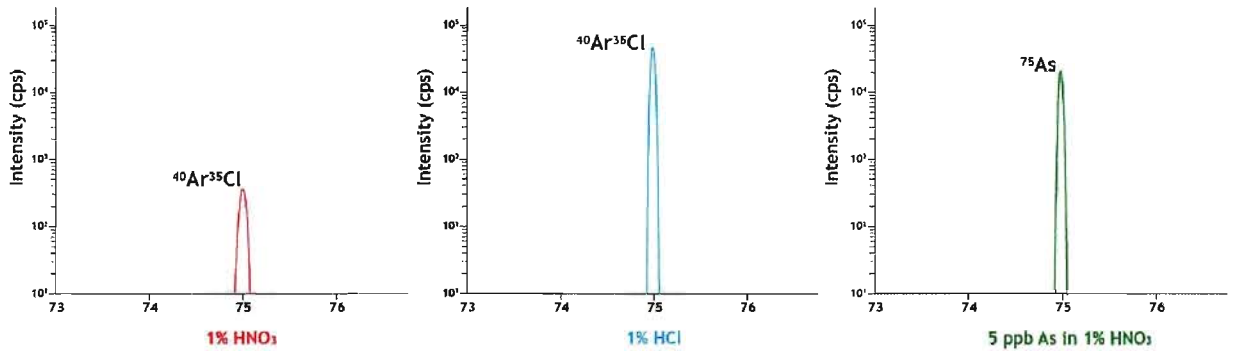

Figure 7. The severity of $ArCl^+$ interference in various matrices.

Although ICP-MS technology literally revolutionized elemental analysis since it first emerged, there were still several elements whose determination by conventional ICP-MS remains ineffective due to severe spectral interferences that are created with plasma gas. Arsenic and selenium fall unfortunately in this group of elements as they are subject to interferences from a range of argon-based polyatomic interferences (see Table 6 for an overview). Entrained in the post-plasma ion beam with analyte ions, these significant molecular ions result directly in

elevated background levels for the listed isotopes, and in some severe cases, will completely swamp the analyte signal if its abundance was relatively low (see Appendix V for a graphical illustration). As to their origins, arsenic suffers largely from a matrix effect because t its major interfering species, $^{40}Ar^{35}Cl^{+}$, depends exclusively on the chloride level in the sample matrix (often derived from the sample preserving and digesting media, such as HCl, see Figure 7). In contrast to the mono-isotopic arsenic, determination of selenium relies on its two relatively abundant isotopes, ^{78}Se and ^{80}Se, which are much less affected by the matrix composition than by the overwhelming argon dimers.

Table 6: A survey of spectral interferences for arsenic and selenium isotopes

Analyte (%)	Isobaric interferences	Polyatomic interferences
^{75}As (100)	-	$^{40}Ar^{35}Cl$, $^{38}Ar^{37}Cl$, $^{40}Ca^{35}Cl$
^{74}Se (0.89)	^{74}Ge (35.94)	$^{38}Ar^{36}Ar$, $^{40}Ar^{34}S$, $^{37}Cl_2$
^{76}Se (9.36)	^{76}Ge (7.44)	$^{40}Ar^{36}Ar$, $^{38}Ar_2$
^{77}Se (7.63)	-	$^{40}Ar^{37}Cl$, $^{40}Ar^{36}ArH$, $^{38}Ar_2H$
^{78}Se (23.78)	^{78}Kr (0.35)	$^{40}Ar^{38}Ar$, $^{38}Ar^{40}Ca$
^{80}Se (49.61)	^{80}Kr (2.25)	$^{40}Ar_2$, $^{40}Ar^{40}Ca$
^{82}Se (8.73)	^{82}Kr (11.6)	$^{40}Ar_2H_2$

Since the high backgrounds of As and Se isotopes in conventional ICP-MS have literally disabled ultra-trace determination for the two elements, other existing measures (mainly cold plasma and sector field high resolution ICP-MS) were also considered. However, their inherent weaknesses often result in poor applicability and robustness. For example, cold plasma ICP-MS

is not suitable for As and Se[l] determination because this technique is fairly inefficient for elements with relatively high ionization potentials (>8eV).[17] Sector field ICP-MS can provide maximum resolution as high as 10,000, slightly greater than the resolutions required to resolve overlapping pairs like $^{75}As^{+}/^{40}Ar^{35}Cl^{+}$ (R=7775) and $^{80}Se^{+}/^{40}Ar_2^{+}$ (R=9688).[81] Nevertheless, its high operating cost and low analyte transmission at such high resolution levels sometimes render sector field ICP-MS unfavorable to meet analyst's needs. Direct measuring of As and Se in standard mode ICP-MS was also documented,[45,82] where the analysts had to live with high background on mass 75 and chose a less-abundant isotope ^{82}Se for quantification, at the cost of significantly compromised analyte sensitiviey. It was not until the introduction of the collision/reaction cell to ICP-MS that such difficulties in arsenic and selenium determination could be alleviated.

Much like the previous case of vanadium determination by ICP-DRC-MS, discussed in Part I, application of a variety of reactive gases has been extensively explored in the past. Ammonia, frequently used in tackling argon-related polyatomic interferences, was not recommended by the manufacturer for the determination of arsenic whereas its use for selenium was conservatively supported. Grotti and Frache[83] experimentally demonstrated its inability towards resolving arsenic due to a dramatic plunge of the As^{+} intensity observed with an increasing of NH_3 gas flow. A recent study by Bohme's group,[84] using SIFT experiments, reported that, under near thermal conditions, ammonia is kinetically very reactive with As and Se through distinctive reaction channels:

$$As^{+} + NH_3 \rightarrow AsNH_2^{+} + H \qquad k = 2.0\times10^{-10}\ cm^3s^{-1} \qquad (12)$$

[l] As (9.7886 eV), Se (9.7524eV).

$$Se^+ + 2NH_3 \rightarrow NH_4^+ + SeNH_2 \qquad k = 1.1\times10^{-11}\ cm^3s^{-1} \qquad (13)^m$$

Methane was also applied in the DRC determination of As and Se. Guo *et al.*[85] reported a near 100% recovery of As in certified reference materials using CH_4 as reaction gas. Pick *et al.*[86] recovered 85% of Se with the same approach. These results reported however are unexpected, due to their non-conformance to the fundamental ion-molecule reaction characteristics described in Bohme's research.[87] CH_4 does remove argon-derived interferences efficiently, but it reacts with As and Se in a rapid manner as well. Its ability to remove the $^{40}Ca^{35}Cl^+$ ion is also less understood. Hence, the validity of employing CH_4 as reaction gas for As and Se analysis is still in controversial territory.

$$As^+ + CH_4 \rightarrow AsCH_2^+ + H_2 \qquad k = 4.8\times10^{-10}\ cm^3s^{-1} \qquad (14)$$

$$Se^+ + CH_4 \rightarrow Se^+(CH_4) \qquad k = 1.5\times10^{-11}\ cm^3s^{-1} \qquad (15)$$

Other approaches investigated previously include using inert gases such as argon or argon/hydrogen mixture, and oxidative gases like oxygen and nitrous oxide.[32,33] So far the exploitation of kinetic properties of inert gases to solve molecular interferences for As and Se has only been qualitatively demonstrated and the resultant limits of detection have not exhibited significant improvement compared with standard mode ICP-MS.[88,89] Strategies using mono-oxidation of arsenic and selenium to form analyte-containing polyatomic ions have been increasingly advocated in recent years[83,86,90,91] as an innovative approach to overcome the persistent plasma-based interferences and matrix effect by chlorides. Olesik *et al.*[33] took advantage of the exothermic reactions of O_2 with As and Se and used a 1% HCl as the matrix for the working standards. The resulting limits of detection were reported in pg mL^{-1} levels,

[m] The corresponding kinetic data refers to the rate-determining step.

suggesting that high chloride in the matrix and argon-related interferences do not contribute to the background with this approach. In Table 7, a thorough interference profile is illustrated for the mass range 91-98 where AsO^+ and SeO^+ ions fall. It can be inferred that, when As and Se are determined in the form of MO (M=As, Se), atomic isobars would play a more influential role on the accuracy of analyte ions, whereas their molecular counterparts are not likely to be present in significant abundances. This could potentially benefit the method detection limit, if the isobaric interferences were handled efficiently.

$$As^+ + O_2 \rightarrow AsO^+ + O \qquad k = 4.0\times10^{-10}\ cm^3s^{-1} \qquad (16)$$

$$Se^+ + O_2 \rightarrow SeO^+ + O \qquad (\Delta H_{rxn} \approx -24\ kJ\ mol^{-1}) \qquad (17)^n$$

Table 7: A survey of spectral interferences for arsenic and selenium mono-oxides

Analyte (%)[o]	Isobaric interferences	Polyatomic interferences[92]
$^{75}As^{16}O$ (100)	^{91}Zr	$^{40}Ar^{35}Cl^{16}O$
$^{74}Se^{16}O$ (0.89)	^{90}Zr (51.45)	$^{40}Ar^{36}Ar^{14}N$
$^{76}Se^{16}O$ (9.36)	^{92}Zr (17.15), ^{92}Mo (14.84)	$^{76}Ge^{16}O$
$^{77}Se\ ^{16}O$(7.63)	^{93}Nb (100)	$^{40}Ar^{37}Cl^{16}O$
$^{78}Se^{16}O$ (23.78)	^{94}Zr (17.38), ^{94}Mo (9.25)	$^{39}K_2{}^{16}O$
$^{80}Se^{16}O$(49.61)	^{96}Zr (2.5), ^{96}Mo (16.68), ^{96}Ru (5.52)	$^{79}Br^{17}O$
$^{82}Se^{16}O$ (8.73)	^{98}Mo (24.13), ^{96}Ru (1.88)	$^{81}Br^{17}O$

[n] Unofficial value used in ref 32, 33. No kinetic rate constant available in current literature.
[o] Refer to the natural abundance of isotopes in per cent forms.

Through an extensive literature review on the topic of arsenic and selenium determination by ICP-DRC-MS, we have carefully evaluated the performance of various candidate reaction gases and concluded that reaction with oxygen to be the most suitable for real-world sample analysis at ng mL^{-1} level. We also realized that many previous studies, especially those dealing with biological and clinical materials, favoured the most abundant $^{80}Se^{16}O^{+}$ as analyte ion without in-depth investigations on the extent and impact of potentially interfering $^{96}Zr^{+}$, $^{96}Mo^{+}$ and $^{96}Ru^{+}$ ions. Though unlikely to be seen in biological forms, Zr, Mo, and Ru do exist (individually or collectively) in certain types of samples, for example, industrial wastewater, sediments, as well as geological materials. Therefore, it is necessary to study their reaction characteristics in the DRC with oxygen gas and develop alternative strategies around those potential spectral nuisances. In the work described in the second half of this thesis, the research efforts were devoted mainly on removal of Zr, Mo and Ru interferences in As and Se measurements in the quest of improved accuracy and detection limits in ultra-trace analysis of the two elements.

Chapter 7: Experimental

7.1 Instrumentation

The instrument used for this project was the same ELAN ICP-DRC-MS described in Chapter Two. The sample introduction system was unchanged as well. Important operating parameters were altered where necessary and are summarized in Table 8.

Table 8. Instrumental settings for ICP-DRC-MS: (As and Se analysis)

Plasma RF power (W)	1300
Plasma gas flow (L min^{-1})	14.5
Auxiliary gas flow (L min^{-1})	1.2
Nebulizer gas flow (L min^{-1})	0.89-0.90 (optimized daily)
Cell gas	Oxygen
Cell gas flow (mL min^{-1})	0.6 (As), 1.25 (Se)
RPa	0 for all analytes
RPq	0.4 (As), 0.65 (Se)
Sample uptake (mL min^{-1})	~1.0
Interface	Pt sampler and skimmer cones
Auto lens calibration	On (Be 6.75V, Co 7.75V, In 8.75V)
Analog Stage Voltage (V)	-2000
Pulse Stage Voltage (V)	1100
Cell Rod Offset Std (V)	-10.00
Discriminator Threshold (mV)	70.00
Cell Path Voltage Std (V)	-15.00
Axial Field Voltage (V)	250.00
Detector	Dual
Scanning mode	Peak hopping
Mathematical correction	None
Dwell time (ms)	150
Sweeps	3
Replicate	3

7.2 Reagents

Research grade plasma gas and cell gas (oxygen) were supplied by Praxair (Hamilton, ON, Canada). Relevant reagent information for this project is supplemented in Appendix II.

7.3 Sample collection and preparation

Seven sludge samples were taken from different wastewater treatment plants in the Niagara Region of Southern Ontario, including one duplicate, and were prepared with a standard *aqua* leach. These samples contain considerable organic content and are intended to be land-applied if the concentrations of pollutants are below regulated levels. Each sample was air-dried at 30 °C and about 0.5 g of each sample and certified reference material was weighed for digestion. The sample digestate was formed in the same manner as for sediment digestion described in Part I (to a final volume of 50 mL). Using a further dilution factor of 50 (for As) or 10 (for Se), two sets of diluted sample were then prepared with 0.5% (m/v) nitric acid. The density of digestates is pooled at 1.013±0.004 g/ml. Therefore, at the designated dilution level, the density correction factor is only about 0.3% and would not give rise to significant bias of the measurements.

7.4 Internal standardization and calibration

The employment of an internal standard (IS) in ICP-MS practices is intended to counteract the non-spectral effects caused by the solid build-up in the sample introduction system, RF ICP instability, as well as instrumental drift. For the sake of analyte stability during hours-long analysis, the use of an internal standard was considered appropriate because, for elements like As and Se whose first ionization potential are relatively high, their signal intensities often exhibit high variations in response to small fluctuations in ICP power. According to USEPA's guidelines[93] and previous experience,[89] Rh, In, and Ir were qualified candidates as 1) they are either not present in samples or resistant to *aqua regia* digestion;[94] 2) they do not react with oxygen under thermal conditions; and 3) they are either similar with the analytes by mass or by first ionization potential (Table 9).

Table 9: Physical properties of candidate internal standards

Element	Atomic/Molecular Mass	1st Ionization Energy[95] (eV)	Reactivity with O_2
As/AsO	75/91	9.789	-
Se/SeO	74-82/90-98	9.752	-
Rh	103	7.459	NR
In	115	5.786	NR
Ir	193	8.967	NR

A solution containing 5 ng mL^{-1} of As, 10 ng mL^{-1} of Se, and 1 ng mL^{-1} of Rh, In, and Ir were run for 2.5 hours in DRC mode for three consecutive days and the performance of three candidate ISs was documented for evaluation purposes. The experimental results showed consistency, in that the analyte signals drifts least with Rh as internal standard (Table 10). The data also implied a more positive impact of difference in mass between analyte and IS ions than the difference in their ionization potential, as far as the analyte stability is concerned. Subsequently, Rh was chosen as internal standard and 1 ng mL^{-1} of Rh was spiked in all working solutions and diluted samples. Two sets of calibration standards were prepared for determination of As (1, 2, 5, 10, and 20 ng mL^{-1}) and Se (5, 10, 20, 50, 100 ng mL^{-1}) with 0.5% (m/v) nitric acid, respectively. Both calibration curves (Appendix VI) were linear through zero (blank subtracted) and exhibited excellent linearity.

Table 10. Comparison of relative analyte stability with respect to Rh, In, and Ir

Day 1 (min)	AsO 91 (cps)	$^{78}Se^{16}O$ (cps)	$^{80}Se^{16}O$ (cps)	Rh 103 (cps)	In 115 (cps)	Ir 193 (cps)	91/103	91/115	91/193	94/103	94/115	94/193	96/103	96/115	96/193
0	8991	2647	5828	50118	52135	19711	0.17940	0.17246	0.45614	0.05282	0.05077	0.13429	0.11629	0.11179	0.29567
10	9131	2735	5999	50065	51634	20381	0.18238	0.17684	0.44802	0.05463	0.05297	0.13419	0.11982	0.11618	0.29434
20	8867	2684	5879	47756	49101	19618	0.18567	0.18059	0.45198	0.05620	0.05466	0.13681	0.12310	0.11973	0.29967
30	8888	2678	5890	48210	49486	19775	0.18436	0.17961	0.44946	0.05555	0.05412	0.13542	0.12217	0.11902	0.29785
40	8585	2599	5717	45775	46911	18540	0.18755	0.18301	0.46305	0.05678	0.05540	0.14018	0.12489	0.12187	0.30836
50	8715	2655	5845	47058	48109	18899	0.18520	0.18115	0.46114	0.05642	0.05519	0.14046	0.12421	0.12149	0.30928
60	8607	2626	5766	46216	47171	18437	0.18623	0.18246	0.46683	0.05682	0.05567	0.14243	0.12476	0.12224	0.31274
70	8863	2709	5963	48514	49399	19151	0.18269	0.17942	0.46280	0.05584	0.05484	0.14145	0.12291	0.12071	0.31137
80	8709	2659	5851	47899	48917	18627	0.18182	0.17804	0.46755	0.05551	0.05436	0.14275	0.12215	0.11961	0.31411
90	8542	2598	5707	47065	47782	17797	0.18149	0.17877	0.47997	0.05520	0.05437	0.14598	0.12126	0.11944	0.32067
100	8445	2551	5605	46301	47087	17238	0.18239	0.17935	0.48991	0.05510	0.05418	0.14799	0.12106	0.11903	0.32515
110	8293	2531	5557	45619	46170	16735	0.18179	0.17962	0.49555	0.05548	0.05482	0.15124	0.12181	0.12036	0.33206
120	8188	2506	5522	45319	45967	16364	0.18067	0.17813	0.50037	0.05530	0.05452	0.15314	0.12185	0.12013	0.33745
130	8177	2509	5488	45374	46066	16244	0.18021	0.17751	0.50339	0.05530	0.05447	0.15446	0.12095	0.11913	0.33785
mean	8642.9	2620.5	5758.4	47234.9	48281.1	18394.1	0.1830	0.1791	0.4712	0.0555	0.0543	0.1429	0.1219	0.1193	0.3140
stdev	294.6	73.9	164.1	1604.5	1949.5	1335.4	0.0024	0.0026	0.0192	0.0010	0.0012	0.0068	0.0022	0.0026	0.0148
rsd	3.41	2.82	2.85	3.40	4.04	7.26	1.33	1.45	4.07	1.81	2.22	4.76	1.80	2.21	4.73
Day 2 (min)	AsO 91 (cps)	$^{78}Se^{16}O$ (cps)	$^{80}Se^{16}O$ (cps)	Rh 103 (cps)	In 115 (cps)	Ir 193 (cps)	91/103	91/115	91/193	94/103	94/115	94/193	96/103	96/115	96/193
0	8412	2100	4565	47727	51076	15346	0.17625	0.16470	0.54816	0.04460	0.04112	0.13684	0.09565	0.08938	0.29747
10	8610	2174	4715	47786	50745	16202	0.18018	0.16967	0.53142	0.04549	0.04284	0.13418	0.09867	0.09292	0.29101
20	8731	2235	4840	47534	50560	16652	0.18368	0.17269	0.52432	0.04702	0.04420	0.13422	0.10182	0.09573	0.29066
30	8713	2265	4926	47491	50229	16519	0.18347	0.17347	0.52745	0.04769	0.04509	0.13711	0.10372	0.09807	0.29820
40	8625	2257	4944	47404	49999	16296	0.18195	0.17250	0.52927	0.04761	0.04514	0.13850	0.10429	0.09888	0.30339
50	8275	2131	4654	45374	47753	15116	0.18237	0.17329	0.54743	0.04697	0.04463	0.14098	0.10257	0.09746	0.30789
60	8183	2104	4554	45071	47548	14683	0.18156	0.17210	0.55731	0.04668	0.04425	0.14329	0.10104	0.09578	0.31015
70	8050	2064	4494	44726	47097	14277	0.17998	0.17092	0.56384	0.04615	0.04382	0.14457	0.10048	0.09542	0.31477
80	7994	2051	4468	44876	47206	13983	0.17814	0.16934	0.57169	0.04570	0.04345	0.14668	0.09956	0.09465	0.31953
90	8029	2073	4509	45163	47356	13914	0.17778	0.16955	0.57704	0.04590	0.04377	0.14899	0.09984	0.09521	0.32406
100	7891	2017	4393	44656	46643	13425	0.17671	0.16918	0.58778	0.04517	0.04324	0.15024	0.09837	0.09418	0.32723
110	7727	1984	4317	44466	46726	13043	0.17377	0.16537	0.59243	0.04462	0.04246	0.15211	0.09709	0.09239	0.33098
120	7680	1963	4304	44710	47024	12841	0.17177	0.16332	0.59808	0.04391	0.04174	0.15287	0.09626	0.09153	0.33518
130	7216	1869	4064	43726	46052	11763	0.16503	0.15669	0.61345	0.04274	0.04058	0.15889	0.09294	0.08825	0.34549
mean	8152.6	2091.9	4553.4	45765.0	48286.7	14575.7	0.1780	0.1688	0.5621	0.0457	0.0433	0.1442	0.0995	0.0943	0.3140
stdev	444.2	115.2	249.0	1461.9	1791.0	1520.6	0.0052	0.0047	0.0290	0.0015	0.0014	0.0077	0.0032	0.0031	0.0171
rsd	5.45	5.51	5.47	3.19	3.71	10.43	2.91	2.81	5.15	3.24	3.27	5.33	3.24	3.30	5.44
Day 3 (min)	AsO 91 (cps)	$^{78}Se^{16}O$ (cps)	$^{80}Se^{16}O$ (cps)	Rh 103 (cps)	In 115 (cps)	r 193 (cps)	91/103	91/115	91/193	94/103	94/115	94/193	96/103	96/115	96/193
0	8215	2093	4525	56588	63255	14275	0.14517	0.12987	0.57548	0.03699	0.03309	0.14662	0.07996	0.07154	0.31699
10	8615	2208	4775	56154	61644	15792	0.15342	0.13975	0.54553	0.03932	0.03582	0.13982	0.08503	0.07746	0.30237
20	8744	2248	4861	55695	60909	16408	0.15700	0.14356	0.53291	0.04036	0.03691	0.13701	0.08728	0.07981	0.29626
30	8801	2251	4917	56106	61066	16724	0.15686	0.14412	0.52625	0.04012	0.03686	0.13460	0.08764	0.08052	0.29401
40	8688	2246	4901	55538	60347	16404	0.15643	0.14397	0.52963	0.04044	0.03722	0.13692	0.08825	0.08121	0.29877
50	8711	2254	4868	55461	60094	16194	0.15707	0.14496	0.53792	0.04064	0.03751	0.13919	0.08777	0.08101	0.30061
60	8620	2233	4834	55062	59993	15897	0.15655	0.14368	0.54224	0.04055	0.03722	0.14047	0.08779	0.08058	0.30408
70	8637	2242	4816	55097	59298	15659	0.15676	0.14565	0.55157	0.04069	0.03781	0.14318	0.08741	0.08122	0.30755
80	8537	2191	4783	54574	58889	15346	0.15643	0.14497	0.55630	0.04015	0.03721	0.14277	0.08764	0.08122	0.31168
90	8455	2198	4733	54415	58882	15232	0.15538	0.14359	0.55508	0.04039	0.03733	0.14430	0.08698	0.08038	0.31073
100	8373	2172	4721	54592	58557	14886	0.15337	0.14299	0.56247	0.03979	0.03709	0.14591	0.08648	0.08062	0.31714
110	8333	2153	4675	54195	58064	14525	0.15376	0.14351	0.57370	0.03973	0.03708	0.14823	0.08626	0.08051	0.32186
120	8372	2159	4697	54618	58316	14512	0.15328	0.14356	0.57690	0.03953	0.03702	0.14877	0.08600	0.08054	0.32366
130	8308	2148	4657	54025	57668	14332	0.15378	0.14407	0.57968	0.03976	0.03725	0.14987	0.08620	0.08076	0.32494
mean	8529.2	2199.7	4768.8	55151.4	59784.4	15441.9	0.1547	0.1427	0.5533	0.0399	0.0368	0.1427	0.0865	0.0798	0.3093
stdev	185.3	49.4	108.8	793.7	1564.5	837.0	0.0031	0.0039	0.0184	0.0009	0.0012	0.0048	0.0021	0.0026	0.0104
rsd	2.17	2.25	2.28	1.44	2.62	5.42	2.03	2.76	3.32	2.36	3.15	3.39	2.40	3.21	3.36

Chapter 8: Results and discussion

8.1 Selection of arsenic and selenium analyte ion

Where oxygen is used as the reaction gas for As and Se determination, the use of $^{75}As^{16}O^+$ ion is non-debatable due to the mono-isotopic nature of arsenic. However, selenium is unevenly distributed between six isotopes ranging from 0.89% to 49.61% in relative abundance (Table 7). Its most abundant isotope, in the form of $^{80}Se^{16}O^+$, has been used in several previous works[32,33,91]. At m/z 91 and 96, the major concerns for the spectral interferences are ^{91}Zr, ^{96}Zr, ^{96}Mo, and ^{96}Ru ions. The primary reaction characteristics of these elements with oxygen are reported in reference 50:

$$Zr^+ + O_2 \rightarrow ZrO^+ + O \qquad k = 5.0\times10^{-10}\ cm^3s^{-1} \qquad (18)$$

$$Mo^+ + O_2 \rightarrow ZrO^+ + O \qquad k = 7.5\times10^{-11}\ cm^3s^{-1} \qquad (19)$$

$$Ru^+ + O_2 \rightarrow RuO_2^+ \qquad k = 1.7\times10^{-13}\ cm^3s^{-1} \qquad (20)$$

Based on the magnitudes of these kinetic reaction rate constants, it can be seen that reactions 18 and 19 proceed rapidly whereas reaction 20 is rather slow. To check the reaction efficiencies, three running standards, each containing 5 ng mL^{-1} of Zr, 5 ng mL^{-1} of Mo, and 10 ng mL^{-1} of Ru, were run independently in the DRC mode with oxygen gas. Figure 8(a) confirms that the actual reaction profiles correspond to the published ones. Ruthenium fails to respond to the addition of oxygen throughout. Molybdenum intensity is reduced by two orders of magnitude but its intensity at hundreds of cps level at the higher oxygen flow rate indicates that the reaction is indeed not 100% complete at the current flow rate. In contrast with the incomplete reaction of Mo, the Zr signal settles quickly at tens of cps level, comparable to the background generated

from 0.5% HNO_3, as the oxygen flow rate increases to around 0.8 mL min^{-1}, indicating the removal of Zr is essentially complete.

In Figure 8(b) the trend of $^{80}Se^{16}O^+$ ion production is compared with $^{96}Ru^+$ in the DRC. It is not difficult to conclude that mass intensity 96 will be unable to reflect genuine $^{80}Se^{16}O^+$ signal in the presence of Ru. Considering the open access to various sources of contamination of the environment, the chances of encountering Mo and Ru in an environmental sample, though presumably at very low levels, do exist. Furthermore, the methodology developed in this study is intended to be not only a workable approach for environmental samples, but also a matrix-independent solution able to deal with much tougher applications, such as geological samples where elevated levels of Zr, Mo, and Ru are anticipated. Hence, the utilization of $^{80}Se^{16}O^+$ as a selenium analyte would likely produce skewed results if attention is not paid to Mo and Ru levels in samples and an alternative analyte should be explored in this regard.

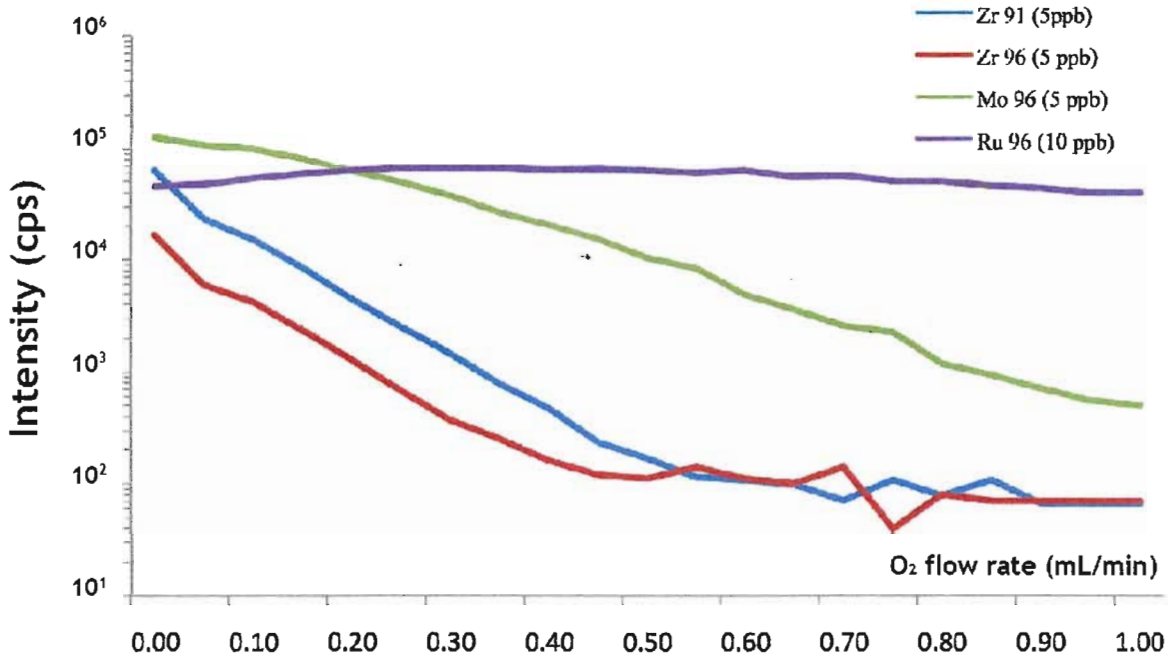

Figure 8(a). Zr 91, Zr 96, Mo 96, and Ru 96 as a function of oxygen gas flow.

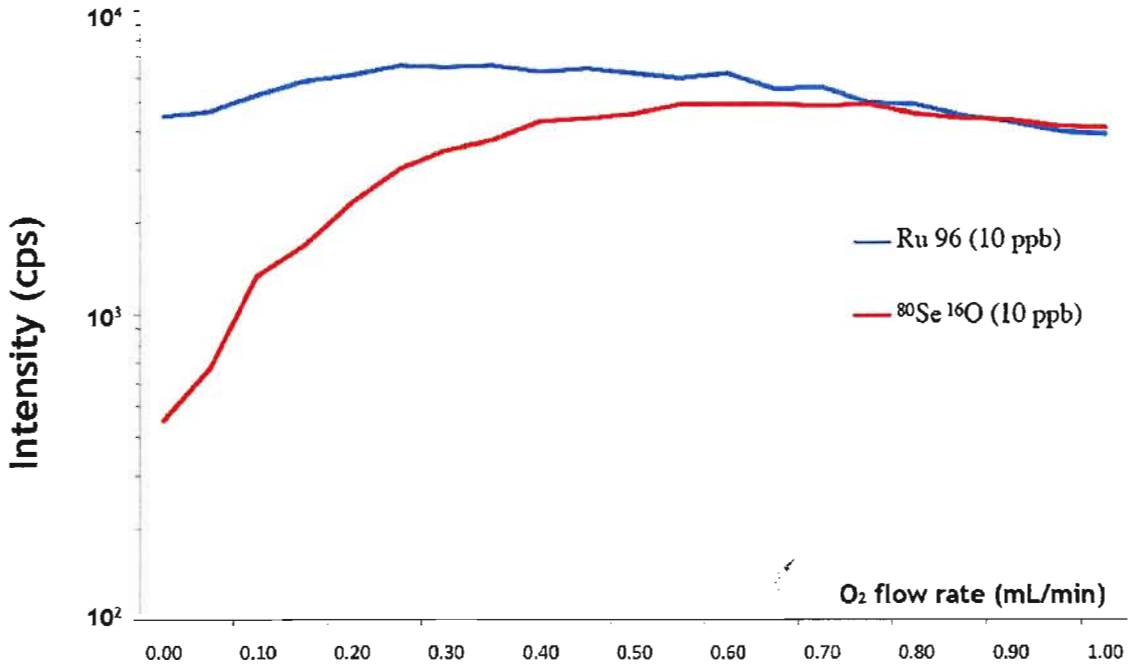

Figure 8(b). SeO (96), Ru 96 as a function of oxygen gas flow.

Conversely, it was noticed that $^{78}Se^{16}O^{+}$ ion overlaps with ^{94}Zr and ^{94}Mo only (Table 7). Although the abundance of ^{78}Se is only about 48% of that of ^{80}Se, it could still maintain an advantage relative to the noise by two orders of magnitude if the Mo interference can be further reduced. Further experiments showed that with a higher oxygen flow rate in the 1.2-1.3 mL min^{-1} range, the ^{94}Mo intensity can be reduced to the tens of cps level while the $^{78}Se^{16}O$ signal remains quite stable (Figure 8 (c)). The robustness of this approach was examined with two levels of Mo (5 ng mL^{-1} and 50 ng mL^{-1}, respectively) and the results, illustrated in Figure 8(c), confirm the effectiveness of the higher oxygen flow rate in reducing interference from ^{94}Mo. Therefore, $^{78}Se^{16}O$ is formally retained in the new method for Se determination in the sludge samples prepared.

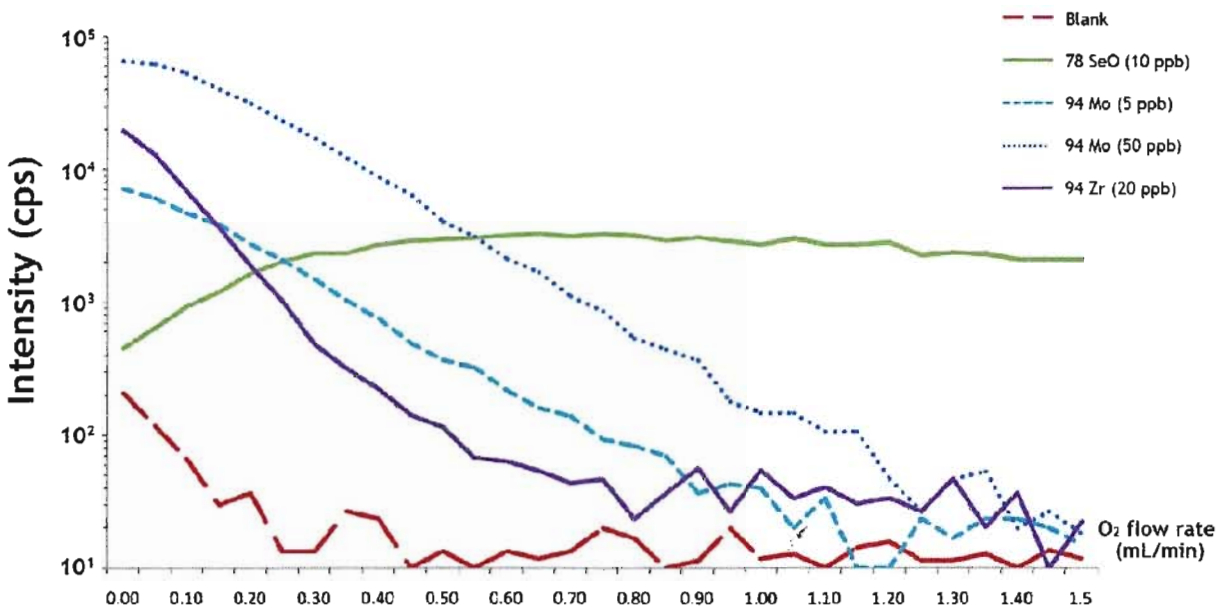

Figure 8(c). SeO (94), Mo 94, and Zr 94 as a function of oxygen gas flow.

8.2 Oxygen gas flow and RPq conditioning

Since $^{75}As^{16}O^{+}$ and $^{78}Se^{16}O^{+}$ are selected for determination, relevant DRC operating parameters must be chosen for generating the optimum signal to noise ratio for each analyte. A blank solution containing 0.5% (v/v) nitric acid and 1% HCl (v/v), and two separate standards, each containing 5 ng mL^{-1} As and 10 ng mL^{-1} Se, were used for optimization purposes. In Figures 9 and 10, the effects of both oxygen gas flow rate and RPq values on analyte intensity and the corresponding detection limit are portrayed. From Figure 9(a) it can be seen that oxygen gas flow rate at 0.5 mL min^{-1} delivers the lowest limit of detection. At this flow rate, however, a two-digit Zr background can not always be guaranteed, depending on its actual concentration in the sample. Therefore, a higher gas flow rate of 0.6 mL min^{-1} was selected for $^{75}As^{16}O^{+}$, where Zr

interference is completely eliminated and the corresponding limit of detection for arsenic is essentially unchanged.

Similar results were obtained for the $^{78}Se^{16}O^{+}$ ion optimization. Initial data suggested that an oxygen gas flow of 0.8 mL min^{-1} results in the lowest detection limit (Figure 10(a)). Considering that a higher gas flow is required to eliminate $^{94}Mo^{+}$ interference, it is necessary to increase the gas flow rate to a point where complete removal of $^{94}Mo^{+}$ and a reasonable $^{78}Se^{16}O^{+}$ detection limit can be simultaneously achieved. As a result, an oxygen flow rate of 1.25 mL min^{-1} was chosen for determination of the analyte as $^{78}Se^{16}O^{+}$. The RPq values most suited for $^{75}As^{16}O^{+}$ and $^{78}Se^{16}O^{+}$ ion are 0.4 and 0.65, respectively. It can be seen from those optimization curves that the limits of detection for arsenic and selenium reached ng L^{-1} and tens of ng L^{-1} levels, thanks to the low backgrounds realized in this higher mass range.

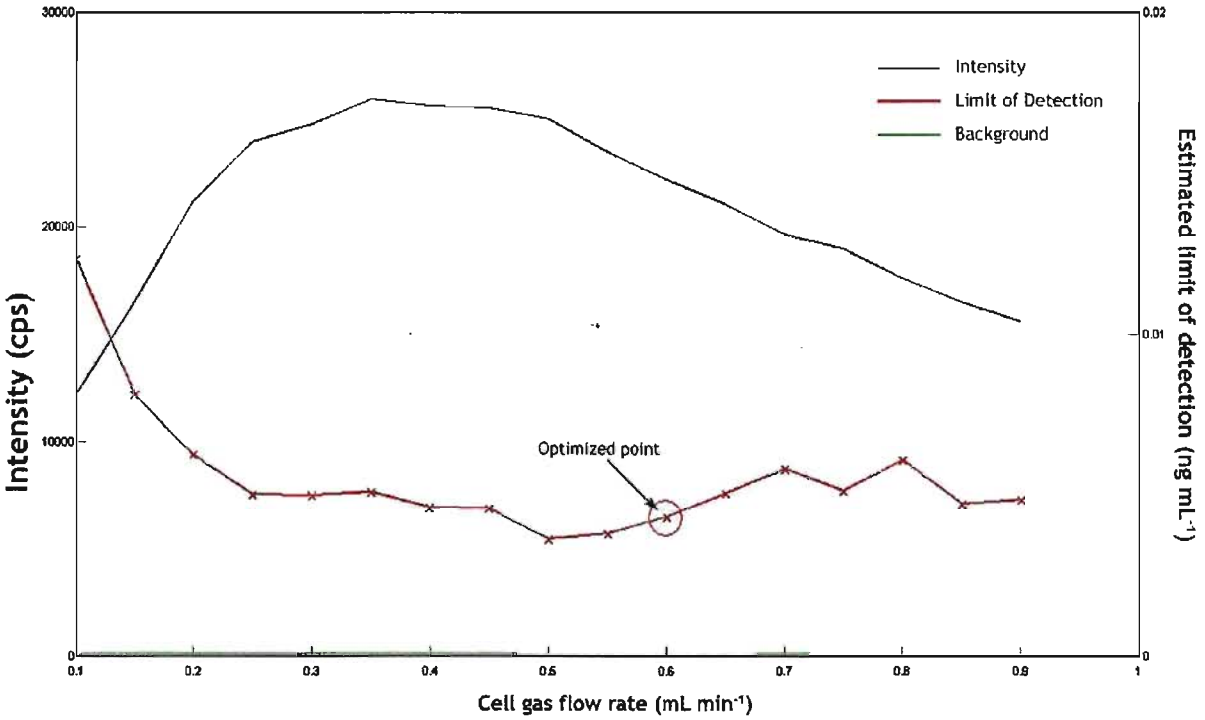

Figure 9(a). Detection limit of $^{75}As^{16}O^{+}$ as a function of oxygen gas flow rate.

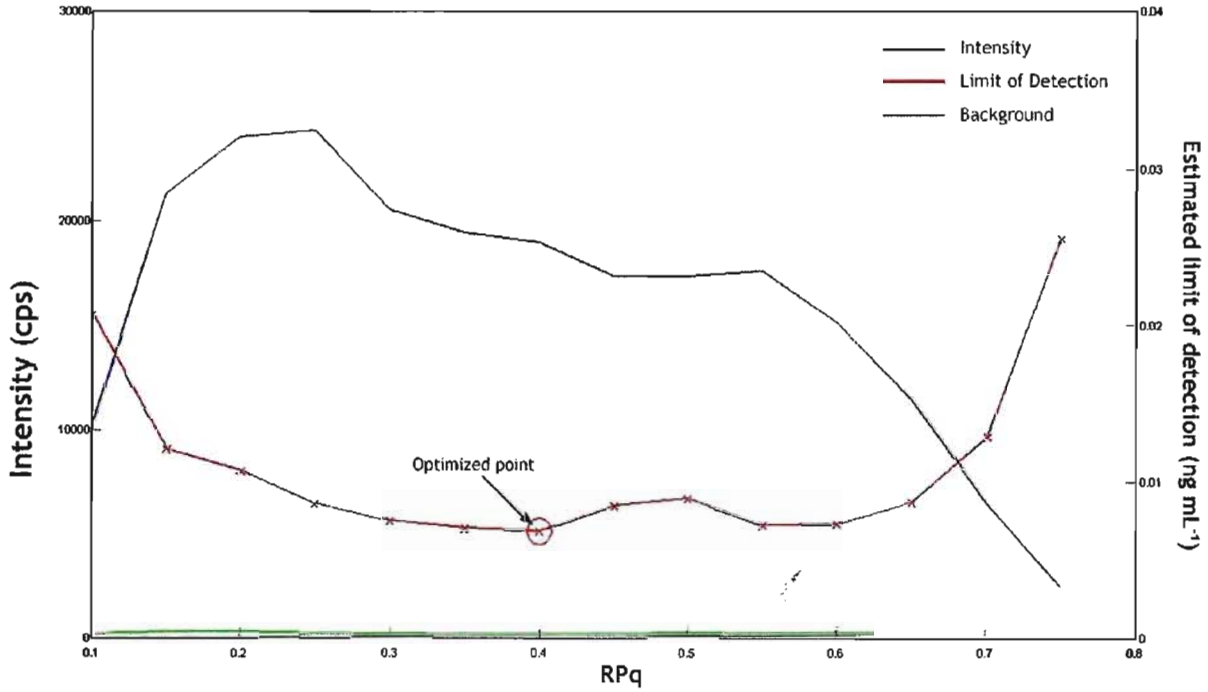

Figure 9(b). Detection limit of $^{75}As^{16}O^{+}$ as a function of RPq.

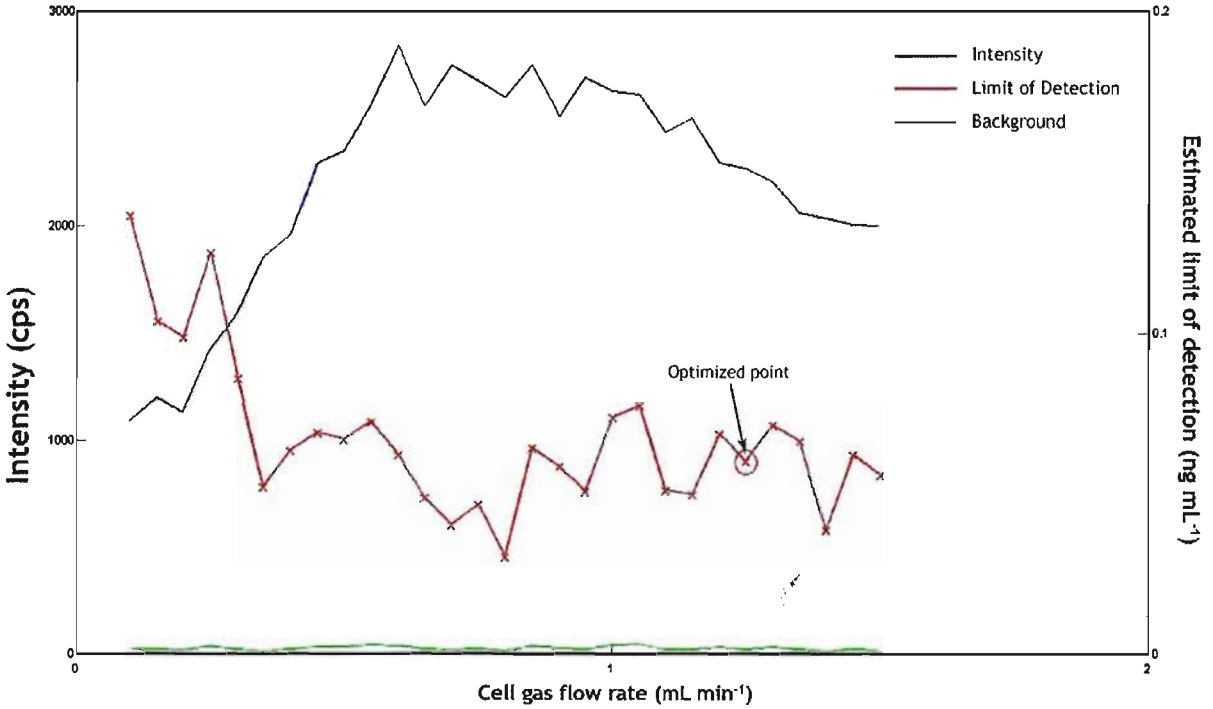

Figure 10(a). Detection limit of $^{78}Se^{16}O^{+}$ as a function of oxygen gas flow rate.

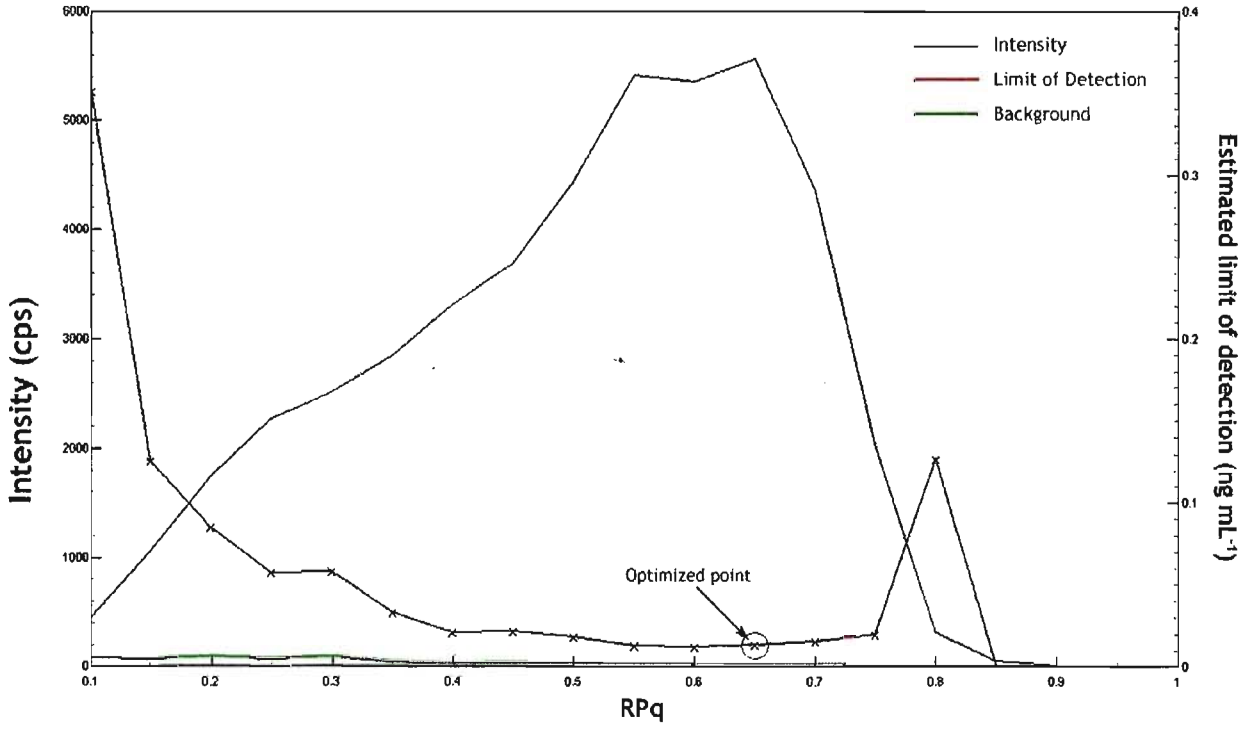

Figure 10(b). Detection limit of $^{78}Se^{16}O^{+}$ as a function of RPq.

8.3 Method validation and analysis of environmental samples

Compared with previous studies that also adopted oxygen as a reaction gas for As and Se determination,[83,86,90,91] a few modifications were made in the current study: a) the impact of Zr^+ on AsO^+ ion was addressed in detail; b) rhodium was selected as internal standard based on a performance assessment of the three candidate isotopes; c) the employment of $^{78}Se^{16}O^+$ ion greatly enhanced the robustness of the method as it relieves the pressure from isobaric interferences from Zr, Mo, and Ru on $^{80}Se^{16}O^+$. Another advantage of the proposed method is that there is no necessity to employ a mathematical equation for interference correction. Consequently, random errors on the measured results can be minimized.

Using cell parameters optimized in Section 7.2, arsenic and selenium results for 7 sludge samples and one certified reference material (CRM031-040-2)[p] are reported in Table 11. Validation of this newly developed method was two-fold. Firstly, the recovery of As and Se in the CRM was evaluated with respect to certified values. A recovery of 100.7% for As and 102.6% for Se was obtained. Secondly, all data obtained from 7 sludge samples were compared with those generated in the Niagara Regional Laboratory, where a standardized HG-ICP-AES method has been employed for routine determination of hydride forming elements. It can be concluded from the good agreement between the two sets of data using paired *t*-tests (Table 12), as well as satisfactory CRM recovery, that the validation of this method is successful.

It should be noted that, despite the good data accuracy achieved, selenium results exhibit relatively large RSDs compared with arsenic. This is probably a direct consequence of the lower sensitivity of $^{78}Se^{16}O^+$ compared with the most abundant $^{80}Se^{16}O^+$ ion. However, paying such a

[p] For verification of trace metal determination in sludge/sediment samples.

price in exchange for confidence in accuracy is often understandable and encouraged in real-world applications, where accuracy of data is the top priority of analysis.

Table 11. Analytical figures of merit for determination of biosolid samples

	ICP-DRC-MS		HG-ICP-AES	
Sample ID	As (mg kg^{-1})[a]	Se (mg kg^{-1})[b]	As (mg kg^{-1})[b]	Se (mg kg^{-1})[b]
51855	$8.8_2 \pm 0.1_1$	$1.1_1 \pm 0.0_3$	$8.5_1 \pm 0.3_7$	$1.1_3 \pm 0.1_6$
81848	$5.2_1 \pm 0.1_3$	$1.1_1 \pm 0.0_4$	$5.1_5 \pm 0.2_9$	$1.0_8 \pm 0.0_2$
81807	$3.8_9 \pm 0.1_0$	$1.1_5 \pm 0.0_5$	$3.5_1 \pm 0.1_1$	$1.5_4 \pm 0.3_8$
53184	$20.5_9 \pm 0.1_6$	$9.9_8 \pm 0.1_2$	$19.0_0 \pm 0.4_3$	$9.7_0 \pm 0.8_2$
53320	$7.0_2 \pm 0.1_4$	$4.0_2 \pm 0.0_7$	$6.9_0 \pm 0.53$	$3.9_0 \pm 0.1_2$
53320-2	$6.5_2 \pm 0.1_3$	$3.7_7 \pm 0.0_7$	$6.6_0 \pm 0.35$	$3.5_0 \pm 0.3_3$
53330	$40.0_6 \pm 0.2_6$	$2.4_1 \pm 0.0_3$	$40.2_0 \pm 1.52$	$2.2_0 \pm 0.0_5$
QC96[c]	$218.3_5 \pm 1.6_8$	$122.1_4 \pm 1.1_2$	$219.0_0 \pm 3.06$	$124.0_0 \pm 1.6_4$
M.R. (%)[d]	100.7	102.6	101.1	104.5
RSD. (%)[e]	0.90-3.03	1.46-4.14	0.91-3.11	0.89-9.80
L.O.D. (ng kg^{-1})[f]	5	60[e]	90	180

a. 1:50 dilution of digestate; b. 1:10 dilution of digestate;

c. Certified value: As 217.0±18.6 mg kg^{-1}, Se 119.0±12.4 mg $kg^{1;}$

d. Method recovery;

e. Relative standard deviation

f. Calculated by ELAN 3.3 software.

Table 12: Paired *t*-tests for As and Se data

	As (ICP-MS) [a]/ As (HG-ICP-AES)[b]	Se (ICP-MS)[b] / Se (HG-ICP-AES)[b]
t(exp)[c]	1.53	0.88

a. 1:50 dilution of digestate; b. 1:10 dilution of digestate; c. Two-tailed $t_{(0.05,7)} = 2.36$

Chapter 9: Conclusion and future prospects

Oxygen has proven to be an excellent reaction gas for accurate determination of total arsenic and selenium in complex environmental samples by ICP-DRC-MS. While abundant chlorine-and-argon based interferences are avoided, conversion of As and Se to AsO and SeO encounters new interference problems due to atomic isobars. Aided with an internal standardization approach, Zr, Mo, and Ru interferences on As and Se are addressed by carefully optimizing DRC operating parameters and selecting an alternative analyte ion, $^{78}Se^{16}O^{+}$. The modified DRC method was successfully validated by good recovery of a certified reference material, as well as inter-laboratory data comparison with a credible analytical institution. Larger standard deviations for selenium, an inherent drawback due to the use of a less abundant selenium isotope, ^{78}Se, were also observed. However, if precision is not the top priority of selenium analysis, the new method is more than capable of delivering both excellent accuracy and limit of detection for ultra-trace determination of the two elements. Our future work on this topic will move on to improving AsO and SeO sensitivities in search of better signal-to-noise ratio. For instance, a few recent studies suggest that addition of organic contents (e.g. methanol) to inorganic solution would likely improve the signal intensity multi-fold.[81,96] This is a very intriguing finding as it could help improve the determination of As and Se at ultra-trace levels. Moreover, application of the current study to more difficult matrices, such as geological samples, could provide a good validation tool to further examine its ability to overcome matrix-induced spectral interferences.

References:

1. S.H. Tan and G. Horlick, *Appl. Spectros.*, 1986, **40**, 445-460.

2. S.J. Hill, *Inductively Coupled Plasma Spectrometry and its Applications 2nd edition*, **2007**, Blackwell Publishing Ltd, Oxford, UK.

3. K.E. Jarvis, A.L. Gray, and R.S. Houk, *Handbook of Inductively Coupled Plasma Mass Spectrometry*, **1992**, Blackie & Son Ltd, Glasgow and London, UK.

4. A. Montaser (Eds.), *Inductively Coupled Plasma Mass Spectrometry*, **1998**, Wiley-VCH Inc., New York, NY, USA.

5. A.L. Gray and J.G. Williams, *J. Anal. At. Spectrom.*, 1987, **2**, 599-606.

6. C. Vandecasteele, and C.B. Block, *Modern Methods for Trace Element Determination*, **1993**, John Wiley & Sons Ltd, West Sussex, UK.

7. K. Hu and R.S. Houk, *J. Amer. Soc. Mass Spectrom.*, 1993, **4**, 28-37.

8. M.A. Vaughan and G. Horlick, *Appl. Spectros.*, 1986, **40**, 434-445.

9. B.T. Ting and M. Janghorbani, *Spectrochimica Acta Part B*, 1987, **42**, 21-27.

10. M.B. Shabani, T. Akagi, H. Shimizu, and A. Masuda, *Anal. Chem.*, 1990, **62**, 2709-2714.

11. S.J. Jiang, M.D. Palmieri, J.S. Fritz, and R.S. Houk, *Anal. Chim. Acta*, 1987, **200**, 559-571.

12. P. Arrowsmith, *Anal. Chem.*, 1987, **59**, 1437-1444.

13. W.T. Buckley, J.J. Budac, D.V. Godfrey, and K.M. Koenig, *Anal. Chem.*, 1992, **64**, 724-729.

14. L.C. Alves, D.R. Wiederin, and R.S. Houk, *Anal. Chem.*, 1992, **64**, 1164-1169.

15. N. Jakubowski, I. Feldmann, and D. Stuewer, *Spectrochim. Acta B*, 1992, **47**, 107-118.

16. E.H. Evans and J.J. Giglio, *J. Anal. At. Spectrom.*, 1993, **8**, 1-18.

17. S.D. Tanner, *J. Anal. At. Spectrom*, 1995, **10**, 905-920.

18. K.E. Javis, *J. Anal. At. Spectrom.*, 1989, **4**, 563-570.

19. D. Potter, *J. Anal. At. Spectrom.*, 2008, **23**, 690-693.

20. R. Thomas, *Spectros.*, 2001, **16**, 44-48.

21. J.T. Rowan and R.S. Houk, *Appl. Spectros.*, 1989, **43**, 976-980.

22. D.J. Douglas, *Can. J. Spectros.*, 1989, **34**, 38-49.

23. D.W. Koppenaal, G.C. Eiden, and C.J. Barinaga, *J. Anal. Atom. Spectrom.*, 2004, **19**, 561-570.

24. S.D. Tanner, V.I. Baranov, and D.R. Bandura, *Spectrochimica Acta B*, 2002, **57**, 1361-1452.

25. V. Chrastný, M. Komárek, M. Mihaljevič, and J. Štíchová, *Anal. Bioanal. Chem.*, 2006, **385**, 962-970.

26. A.J.B. Cotta and J. Enzweiler, *J. Anal. At. Spectrom.*, 2009, **24**, 1406-1413.

27. I. Feldmann, N. Jakubowski, C. Thomas, and D. Stuewer, *Fresen. J. Anal. Chem.*, 1999, **365**, 422-428.

28. V.I. Baranov and S.D. Tanner, *J. Anal. At. Spectrom.*, 1999, **14**, 1133-1142.

29. S.D. Tanner and V.I. Baranov, *J. Am. Soc. Mass Spectrom.*, 1999, **10**, 1083-1094.

30. S.D. Tanner, V.I. Baranov and U. Vollkopf, *J. Anal. At. Spectrom.*, 2000, **15**, 1261-1269.

31. L.A. Simpson, M. Thomsen, B.J. Alloway, and A. Parker, *J. Anal. At. Spectrom.*, 2001, **16**, 1375-1380.

32. B. Hattendorf and D. Günther, *Spectrochimica Acta Part B*, 2003, **58**, 1-13.

33. J.W. Olesik and D.R. Jones, *J. Anal. At. Spectrom.*, 2006, **21**, 141-159.

34. V.G. Anicich, *J. Phys. Chem. Ref. Data*, 1993, **22**, 1469-1569.

35. V.G. Anicich (Eds.), *An index of the literature for biomolecular gas phase cation-molecule reaction kinetics*, **2003**, NASA/Jet Propulsion Laboratory, Report #03-19.

36. York University (Canada)'s kinetics database. Available online at URL: http://www.chem.yorku.ca/profs/bohme/research/selection_table.html (Accessed on April 9, 2011)

37. Y. Wang and I.D. Brindle, *J. Anal. At. Spectrom.*, 2011, **26**, 1514-1520.

38. H. Louie, M. Wu, P. Di, P. Snitch and G. Chapple, *J. Anal. At. Spectrom*, 2002, **17**, 587-589.

39. D.E. Nixon, K.R. Neubauer, S.J. Eckdahl, J.A. Butz and M.F. Burritt, *Spectrochim Acta B*, 2002, **57**, 951- 966.

40. N.M. Reed, R.O. Cairns, R.C. Hutton and Y. Takaku, *J. Anal. At. Spectrom.*, 1994, **9**, 881-896.

41. C-F. Wang, C.Y. Chang, C.J. Chin and L.C. Men, *Anal. Chim. Acta*, 1999, **392**, 299-306.

42. C.C. Chery, K.D. Cremer, R. Cornelis, F. Vanhaecke and L. Moens, *J. Anal. At. Spectrom.*, 2003, **18**, 1113-1118.

43. *S.* D'Ilio, N. Violante, M. Di Gregorio, O. Senofonte and F. Petrucci, *Anal. Chim. Acta*, 2006, **579**, 202-208.

44. M. Grotti, F. Soggia, J.L. Todoli, *Analyst*, 2008, **133**, 1388-1394.

45. B.L. Batista, J.L. Rodrigues, J.A. Nunes, V.C. de Oliveira Souza and F. Barbosa Jr., *Anal. Chim. Acta*, 2009, **639**, 13-18.

46. Y.Y. Chan and S.C.L. Lo, *J. Anal. At. Spectrom.*, 2003, **18**, 146-150.

47. N. Nonose, M. Ohata, T. NAarukawa, A. Hioki and K. Chiba, *J. Anal. At. Spectrom.*, 2009, **24**, 310-319.

48. D.E. Clemmer, L.S. Sunderlin, and P.B. Armentrout, *J. Phys. Chem.*, 1990, **94**, 208-217.

49. J.w. Olesik, C. Hensman, S. Rabb and D. Rago, in *Plasma Source Mass Spectrometry: The New Millenium*, G. Holland and S.D. Tanner (Eds.), **2001**, the Royal Society of Chemistry, Cambridge, UK.

50. G.K. Koyanagi, D. Caraiman, V. Blagojevic and D.K. Bohme, *J. Phys. Chem. A*, 2002, **106**, 4581-4590.

51. V.V. Lavrov, V. Blagojevic, G.K. Koyanagi and D.K. Bohme, *J. Phys. Chem. A*, 2004, **108**, 5610-5624.

52. V. Blagojevic, E. Flaim, M.J.Y. Jarvis, G.K. Koyanagi and D.K. Bohme, *J. Phys. Chem. A*, 2005, **109**, 11224-11235.

53. P. Cheng, G.K. Koyanagi, and D.K. Bohme, *J. Phys. Chem. A*, 2006, **110**, 2718-2728.

54. X. Zhao, G.K. Koyanagi, and D.K. Bohme, *J. Phys. Chem. A*, 2006, **110**, 10607-10618.

55. G.K. Koyanagi, V.I. Baranov, S.D. Tanner and D.K. Bohme, *J.Anal. At. Spectrom.*, 2000, **15**, 1207-1210.

56. D.R. Bandura, V.I. Baranov, and S.D. Tanner, *Fresen. J. Anal. Chem.*, 2001, **370**, 454-470.

57. A.J. Bednar, *Talanta*, 2009, **78**, 453-457.

58. N. Kalogeropoulos, M. Scoullos, M. Vassilaki-Grimani and A.P. Grimanis, *The scien. of the Total Envi.*, 1989, **79**, 241-252.

59. M. Colina, P.H.E. Gardiner, Z. Rivas and F. Troncone, *Analytica Chimica Acta*, 2005, **538**, 107-115.

60. G.K. Koyanagi, D.K. Bohme, I. Kretzschmar, D. Schröder, and H. Schwarz, *J. Phys. Chem. A*, 2001, **105**, 4259-4271.

61. T. Kaya, M. Kobayashi, H. Shinohara and H. Sato, *Chem. Phys. Letters*, 1991, **186**, 431-435.

62. US EPA method 6020. Available online at URL: http://servicio.us.es/sgiaus/Nuevo-Sia/Metodos/EPA6020.pdf (Accessed on April 10, 2011)

63. S. Aries, M. Valladon, M. Polve and B. Dupre, *Geostandards Newsletter*, 2000, **24**, 19-31.

64. M. Colon, M. Hidalgo and M. Iglesias, *J.Anal. At. Spectrom.*, 2009, **24**, 518-521.

65. P.B. Armentrout, L.F. Halle, and J.L. Beauchamp, *J. Chem. Phys.*, 1982, **76**, 2449-2457.

66. S. Mahimairaja, N.S. Bolan, D.C. Adriano and B. Robinson, *Advances in Agronomy*, 2005, **86**, 1.

67. C.G. Wilber, *Selenium: A Potential Environmental Poison and a Necessary Food Constituent*, **1983**, Charles C Thomas Publisher, Springfield, Illinois, USA.

68. S. Hirata and H. Toshimutsu, *Appl. Organo. Chem.*, 2007, **21**, 447.

69. J.E. Conde and M.S. Alaejos, *Chem. Rev.*, 1997, **97**, 1979-2003.

70. S. Pansamut and G. Wattayakorn, *Enviro. Research and Development*, 2009, **3**, 607.

71. A-K Malik, M. Gomez, C. Camara, H-G Riepe and J. Bettmer, *Inter. J. Environ. Anal. Chem.*, 2002, **82**, 795.

72. Y-J Tseng, C-C Liu, S-J Jiang, *Anal. Chim. Acta*, 2007, **588**, 173.

73. Technical Support Document for Ontario Drinking Water Standards, Objectives, and Guidelines, Rev. **2006**. Available online at URL: http://www.ene.gov.on.ca/environment/fr/resources/STD01_077338.html (Accessed on May 18, 2011).

74. Ontario Nutrient Management Act, **2002**. Available online at URL: http://www.e- laws.gov.on.ca/html/regs/english/elaws_regs_030267_e.htm (Accessed on May 18, 2011)

75. M. Veber, K. Cujes, and S. Gomiscek, *J.Anal. At. Spectrom.,* 1994, **9**, 285-290.

76. H. Chen, I.D. Brindle, and X-C Le, *Anal. Chem.*, 1992, **64**, 667-672.

77. I.D. Brindle and E. Lugowska, *Spectrochim Acta B*, 1997, **52**, 163-176.

78. P. Schramel and L-Q Xu, *Fresenius J. Anal.Chem.*, 1991, **340**, 41-47.

79. P. Bermejo, J. Moreda, A. Moreda, and A. Bermejo, *Fresenius J. Anal. Chem.*, 1996, **355**, 174-179.

80. Y-Z Liang, M. Li, and Z. Rao, *Fresenius J. Anal.Chem.*, 1997, **357**, 112-116.

81. N. Jakubowski, L. Moens, and F. Vanhaecke, *Spectrochim Acta B*, 1998, **53**, 1739-1763.

82. S. D'Ilio, F.Petrucci, M. D'Amato, M. Di Gregorio, O. Senofonte, and N. Violante, *Analytica Chimica Acta*, 2008, **624**, 59-67.

83. M. Grotti and R. Frache, *J.Anal. At. Spectrom.,* 2007, **22**, 1481-1487.

84. G.K. Koyanagi, V. Kapishon, D.K. Bohme, X-H. Zhang, and H. Schwarz, *Eur. J. Inorg. Chem.*, 2010, **15**16-1521.

85. W. Guo, S-H. Hu, X-F. Li, J. Zhao, S-S. Jin, W-J. Liu, and H-F. Zhang, *Talanta*, 2011, **84**, 887-894.

86. D. Pick, M. Leiterer, and J.W. Einax, *Microchem. J.*, 2010, **95**, 315-319.

87. A. Shayesteh, V.V. Lavrov, G.K. Koyanagi, and D.K. Bohme, *J. Phys. Chem. A*, 2009, **113**, 5602-5611.

88. D.E. Nixon, K.R. Neubauer, S.J. Eckdahl, J.A. Butz, and M.F. Burritt, *Spectrochim Acta B*, 2004, **59**, 1377-1387.

89. W.J. McShane, R.S. Pappas, and D. Paschal, *J.Anal. At. Spectrom.,* 2007, **22**, 630-635.

90. J-K. Suh, N-G. Kang, and J-B. Lee, *Talanta*, 2009, **78**, 321-325.

91. S. Sturup, L. Bendahl, and B. Gammelgaard, *J.Anal. At. Spectrom.,* 2006, **21**, 201-203.

92. T.W. May and R.H. Wiedmeyer, *Atom. Spectros.*, 1998, **19**, 150-155.

93. USEPA Method 200.8. Available online at URL: http://www.dec.state.ak.us/eh/docs/lab/dw/Chem/inorganics/200.8.pdf (Accessed on May 18, 2011)

94. C.E. Housecroft, A.G. Sharpe, *Inorganic Chemistry (2nd edition)*, 2005, Prentice Hall, New York, USA.

95. NIST Ground levels and ionization energies for the neutral atoms. Available online at URL: http://physics.nist.gov/PhysRefData/IonEnergy/tblNew.html (Accessed on Apr 8, 2011)

96. J.M. Jarrett, R.L. Jones, K.L. Caldwell, and C.P. Verdon, *Atom. Spectros.*, 2007, **28**, 113-119.

Appendix I: A table of natural isotopic abundances

Isotope		%		%		%
1	H	99.985				
2	H	0.015				
3			He	0.000137		
4			He	99.999863		
5						
6					Li	7.5
7					Li	92.5
8						
9	Be	100				
10			B	19.9		
11			B	80.1		
12					C	98.90
13					C	1.10
14	N	99.643				
15	N	0.366				
16			O	99.762		
17			O	0.038		
18			O	0.200		
19					F	100
20	Ne	90.48				
21	Ne	0.27				
22	Ne	9.25				
23			Na	100		
24					Mg	78.99
25					Mg	10.00
26					Mg	11.01
27	Al	100				
28			Si	92.23		
29			Si	4.67		
30			Si	3.10		
31					P	100
32	S	95.02				
33	S	0.75				
34	S	4.21				
35			Cl	75.77		
36	S	0.02			Ar	0.337
37			Cl	24.23		
38					Ar	0.063
39	K	93.2581				
40	K	0.0117	Ca	96.941	Ar	99.600
41	K	6.7302				
42			Ca	0.647		
43			Ca	0.135		
44			Ca	2.086		
45					Sc	100
46	Ti	8.0	Ca	0.004		
47	Ti	7.3				
48	Ti	73.8	Ca	0.187		
49	Ti	5.5				
50	Ti	5.4	V	0.250	Cr	4.345
51			V	99.750		
52					Cr	83.789
53					Cr	9.501
54	Fe	5.9			Cr	2.365
55			Mn	100		
56	Fe	91.72				
57	Fe	2.2				
58	Fe	0.28			Ni	68.077
59			Co	100		
60					Ni	26.223

Isotope		%		%		%
61					Ni	1.140
62					Ni	3.634
63	Cu	69.17				
64			Zn	48.6	Ni	0.926
65	Cu	30.83				
66			Zn	27.9		
67			Zn	4.1		
68			Zn	18.8		
69					Ga	60.108
70	Ge	21.23	Zn	0.6		
71					Ga	39.892
72	Ge	27.66				
73	Ge	7.73				
74	Ge	35.94	Se	0.89		
75					As	100
76	Ge	7.44	Se	9.36		
77			Se	7.63		
78	Kr	0.35	Se	23.78		
79					Br	50.69
80	Kr	2.25	Se	49.61		
81					Br	49.31
82	Kr	11.6	Se	8.73		
83	Kr	11.5				
84	Kr	57.0	Sr	0.56		
85					Rb	72.165
86	Kr	17.3	Sr	9.86		
87			Sr	7.00	Rb	27.835
88			Sr	82.58		
89					Y	100
90	Zr	51.45				
91	Zr	11.22				
92	Zr	17.15	Mo	14.84		
93					Nb	100
94	Zr	17.38	Mo	9.25		
95			Mo	15.92		
96	Zr	2.80	Mo	16.68	Ru	5.52
97			Mo	9.55		
98			Mo	24.13	Ru	1.88
99					Ru	12.7
100			Mo	9.63	Ru	12.6
101					Ru	17.0
102	Pd	1.02			Ru	31.6
103			Rh	100		
104	Pd	11.14			Ru	18.7
105	Pd	22.33				
106	Pd	27.33	Cd	1.25		
107					Ag	51.839
108	Pd	26.46	Cd	0.89		
109					Ag	48.161
110	Pd	11.72	Cd	12.49		
111			Cd	12.80		
112	Sn	0.97	Cd	24.13		
113			Cd	12.22	In	4.3
114	Sn	0.65	Cd	28.73		
115	Sn	0.34			In	95.7
116	Sn	14.53	Cd	7.49		
117	Sn	7.68				
118	Sn	24.23				
119	Sn	8.59				
120	Sn	32.59	Te	0.096		

Isotope		%		%		%
121					Sb	57.36
122	Sn	4.63	Te	2.603		
123			Te	0.908	Sb	42.64
124	Sn	5.79	Te	4.816	Xe	0.10
125			Te	7.139		
126			Te	18.95	Xe	0.09
127	I	100				
128			Te	31.69	Xe	1.91
129					Xe	26.4
130	Ba	0.106	Te	33.80	Xe	4.1
131					Xe	21.2
132	Ba	0.101			Xe	26.9
133			Cs	100		
134	Ba	2.417			Xe	10.4
135	Ba	6.592				
136	Ba	7.854	Ce	0.19	Xe	8.9
137	Ba	11.23				
138	Ba	71.70	Ce	0.25	La	0.0902
139					La	99.9098
140			Ce	88.48		
141					Pr	100
142	Nd	27.13	Ce	11.08		
143	Nd	12.18				
144	Nd	23.80	Sm	3.1		
145	Nd	8.30				
146	Nd	17.19				
147			Sm	15.0		
148	Nd	5.76	Sm	11.3		
149			Sm	13.8		
150	Nd	5.64	Sm	7.4	†	
151					Eu	47.8
152	Gd	0.20	Sm	26.7		
153					Eu	52.2
154	Gd	2.18	Sm	22.7		
155	Gd	14.80				
156	Gd	20.47	Dy	0.06		
157	Gd	15.65				
158	Gd	24.84	Dy	0.10		
159					Tb	100
160	Gd	21.86	Dy	2.34		
161			Dy	18.9		
162	Er	0.14	Dy	25.5		
163			Dy	24.9		
164	Er	1.61	Dy	28.2		
165					Ho	100
166	Er	33.6				
167	Er	22.95				
168	Er	26.8	Yb	0.13		
169					Tm	100
170	Er	14.9	Yb	3.05		
171			Yb	14.3		
172			Yb	21.9		
173			Yb	16.12		
174			Yb	31.8	Hf	0.162
175	Lu	97.41				
176	Lu	2.59	Yb	12.7	Hf	5.206
177					Hf	18.606
178					Hf	27.297
179					Hf	13.629
180	Ta	0.012	W	0.13	Hf	35.100

Isotope		%		%		%
181	Ta	99.988				
182					W	26.3
183					W	14.3
184	Os	0.02			W	30.67
185						
186	Os	1.59	W	28.6		
187	Os	1.6			Re	62.60
188	Os	13.3				
189	Os	16.1				
190	Os	26.4				
191					Ir	37.3
192	Os	41.0				
193					Ir	62.7
194						
195						
196	Hg	0.15				
197					Au	100
198	Hg	9.97				
199	Hg	16.87				
200	Hg	23.10				
201	Hg	13.18				
202	Hg	29.86				
203						
204	Hg	6.87	Pb	1.4		
205						
206			Pb	24.1		
207			Pb	22.1		
208			Pb	52.4		
209	Bi	100				
210						
211						
212						
213						
214						
215						
216						
217						
218						
219						
220						
221						
222						
223						
224						
225						
226						
227						
228						
229						
230						
231	Pa	100				
232	Th	100				
233						
234	U	0.0055				
235	U	0.7200				
236						
237						
238	U	99.2745				

Appendix II: Reagents and standards information

Concentrated Nitric Acid: LOT # 50781 (Caledon Lab Chemicals)

Concentrated Hydrochloric Acid: LOT # 68401 (Caledon Lab Chemicals)

Vanadium Stock Solution: LOT# 0916217 (High-Purity Standards, 1000 ppm)

Zinc Stock Solution: LOT# 0916202 (High-Purity Standards, 1000 ppm)

Magnesium Stock Solution: LOT# 0919727 (High-Purity Standards, 1000 ppm)

Indium Stock Solution: LOT# 0920942 (High-Purity Standards, 1000 ppm)

Uranium Stock Solution: LOT# 0921112 (High-Purity Standards, 1000 ppm)

Cerium Stock Solution: LOT# 0916809 (High-Purity Standards, 1000 ppm)

Barium Stock Solution: LOT# 0911910 (High-Purity Standards, 1000 ppm)

Arsenic Stock Solution: Lot# 0919418 (High-Purity Standards, 1000 ppm)

Selenium Stock Solution: Lot# 1019712 (High-Purity Standards, 1000 ppm)

Rhodium Stock Solution: Lot# 0916722 (High-Purity Standards, 1000 ppm)

Iridium Stock Solution: made from "Bis-(1,5-cyclooctadiene)-diiridium(I)-dichloride" (97%) powder, Sigma-Aldrich, USA.

Zirconium Stock Solution: made from "Bis-cyclopentadienyl-zirconium-dichloride" (99%) powder, STREM Chemicals, USA.

Molybdenum Stock Solution: Lot# 0833104 (High-Purity Standards, 100 ppm)

Ruthenium Stock Solution: made from "Ruthenium (III) chloride" powder, Sigma-Aldrich, USA

CRM031-040-1: Lot#012211 (RTC, Laramie, WY, USA)

CRM031-040-2: Lot# 014679 (RTC, Laramie, WY, USA)

Appendix III: Calibration curves for vanadium determination

1. NH_3 as reaction gas (calibration range 0-20 ng mL^{-1})

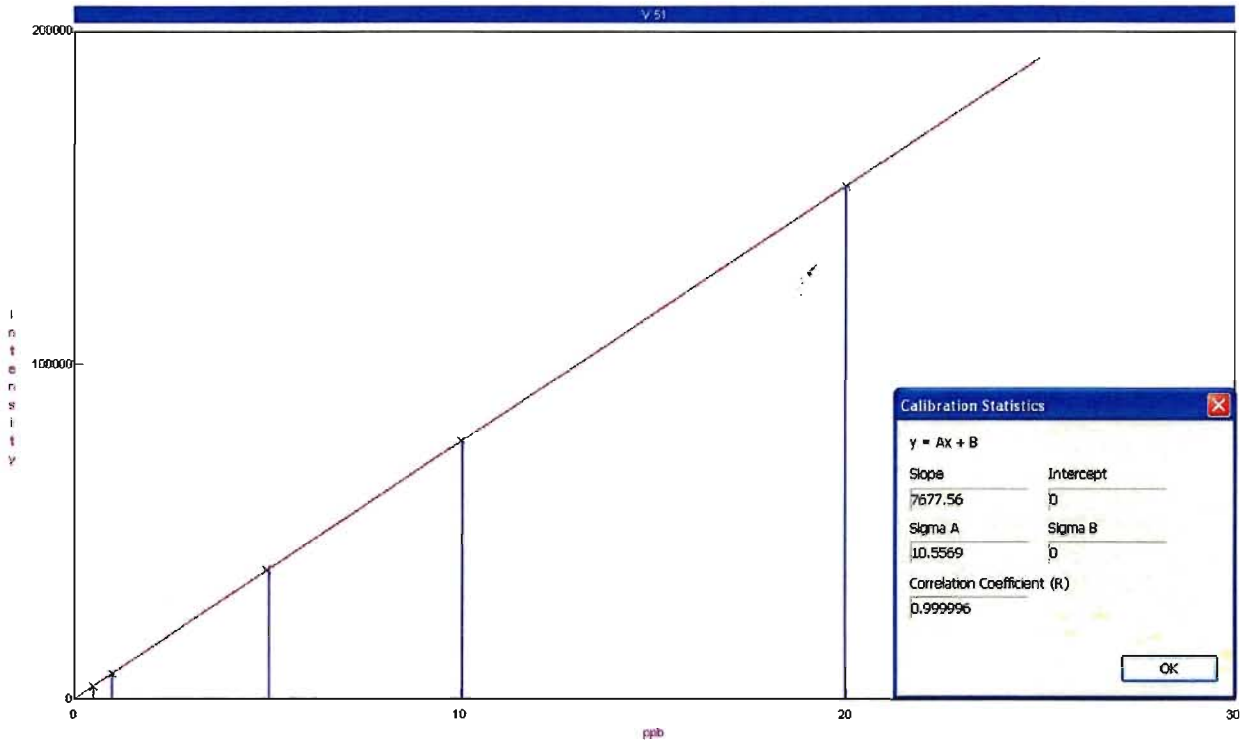

Appendix III-continued

2. NH_3 as reaction gas (calibration range 0-2000 pg mL^{-1})

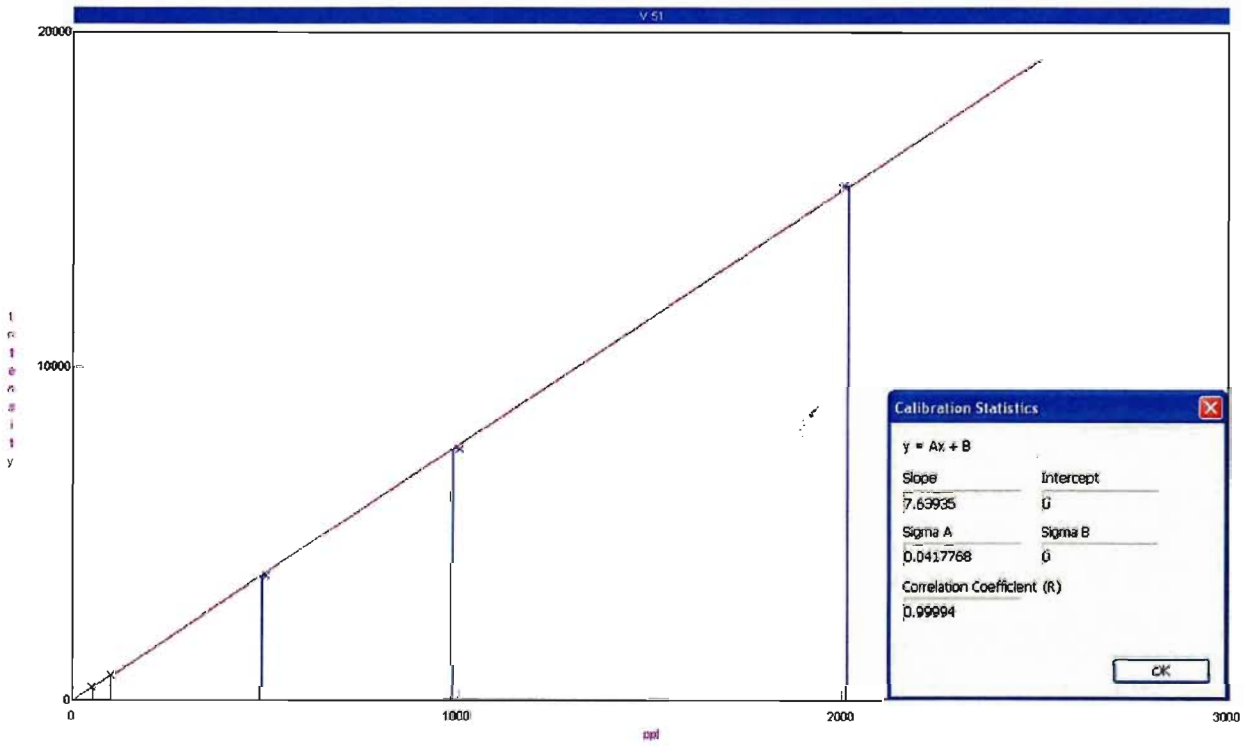

Appendix III- continued

3. O_2 as reaction gas (calibration range 0-20 ng mL^{-1})

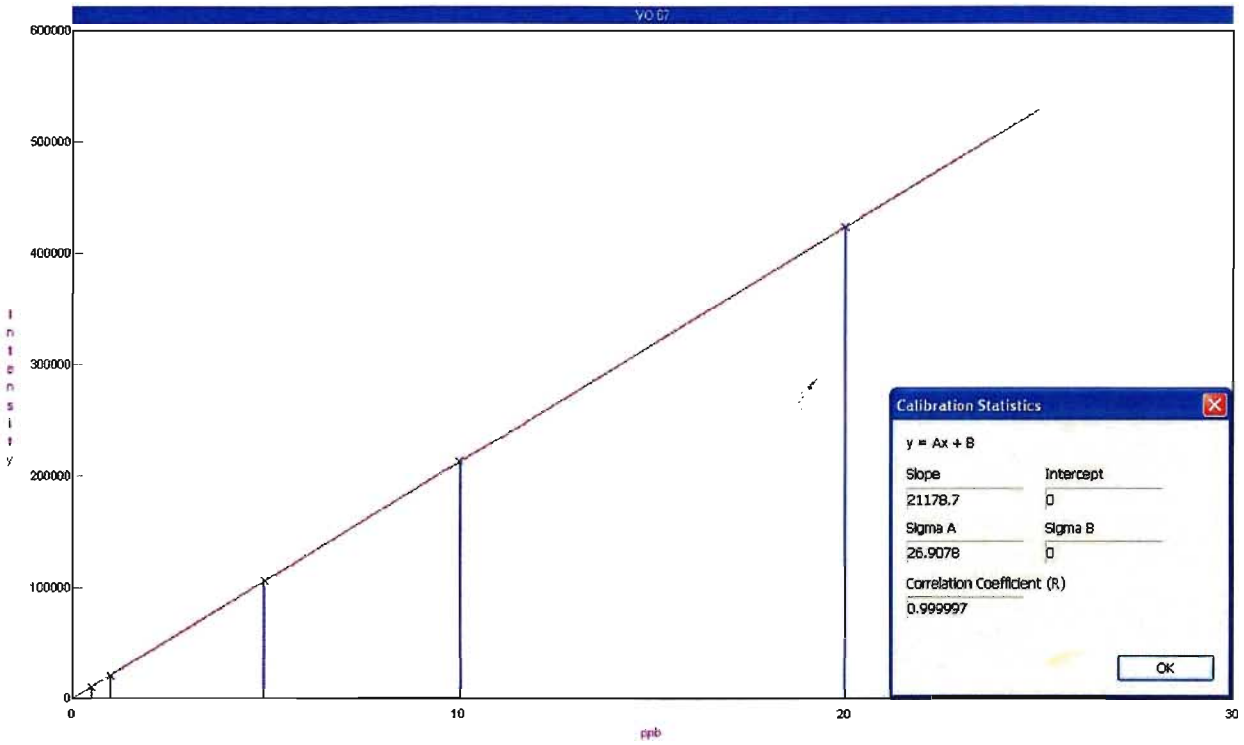

Appendix III- continued

4. N_2O as reaction gas (calibration range 0-20 ng mL^{-1})

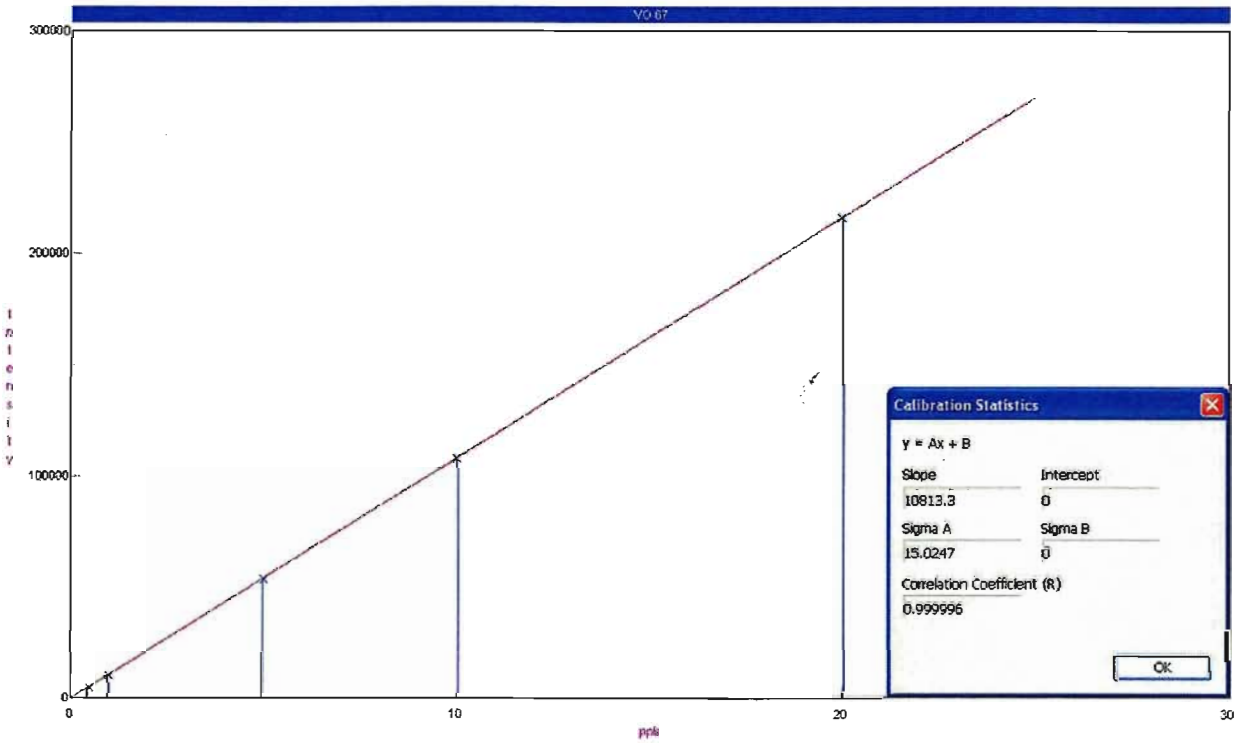

Appendix IV: A partial list of environmental regulations on As and Se

Regulation	Year	Maximum level (mg/Kg, mg/L)	
		As	Se
Ontario drinking water standards, objectives, and guidelines	**2006**	**0.025**	**0.01**
Ontario nutrient management Act	**2002**	**14 (in soil)**	**1.6 (in soil)**
Guidelines for Canadian drinking water quality	**2010**	**0.01**	**0.01**
US Safe drinking water Act	**1996**	**0.01**	**0.05**
WHO Guidelines for drinking-water quality	**2008**	**0.01**	**0.01**

Appendix V: Analyte and background intensities for As and Se

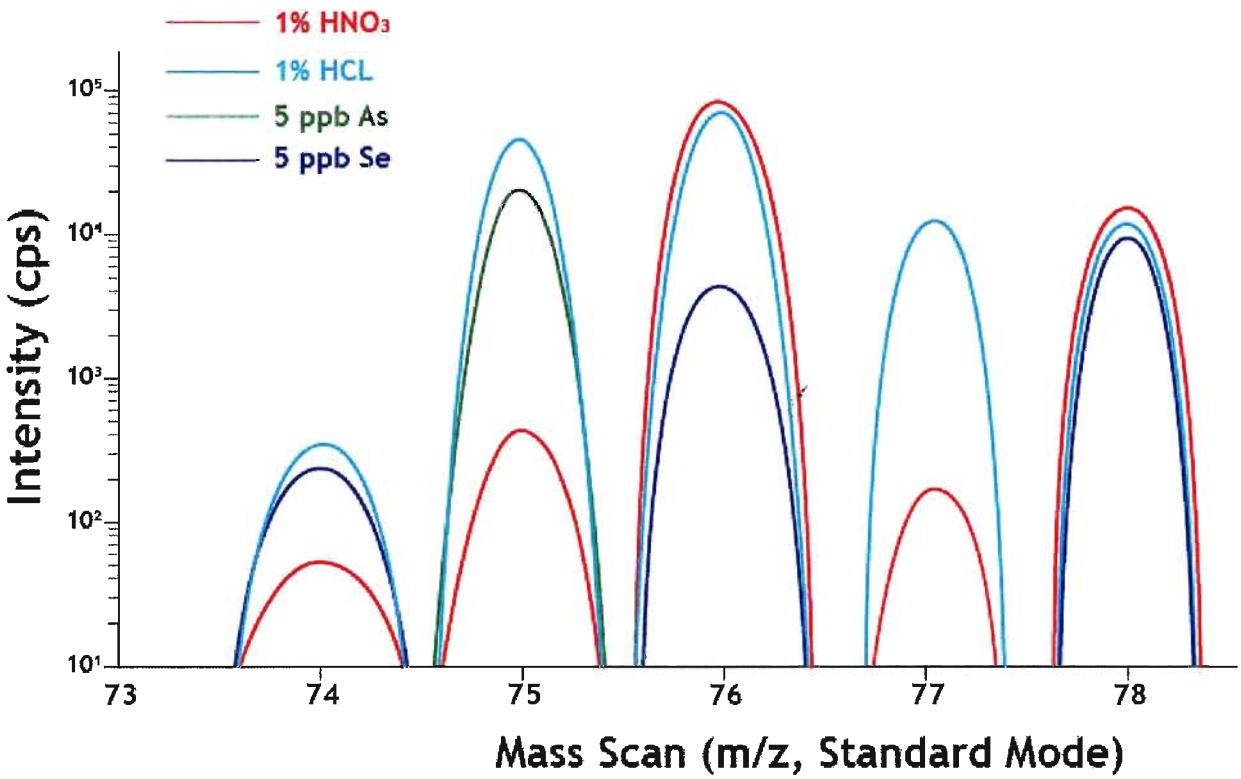

Appendix VI: Calibration curves for arsenic and selenium determination

1. O_2 as reaction gas to produce $^{75}As^{16}O$ (calibration range 0-20 ppb)

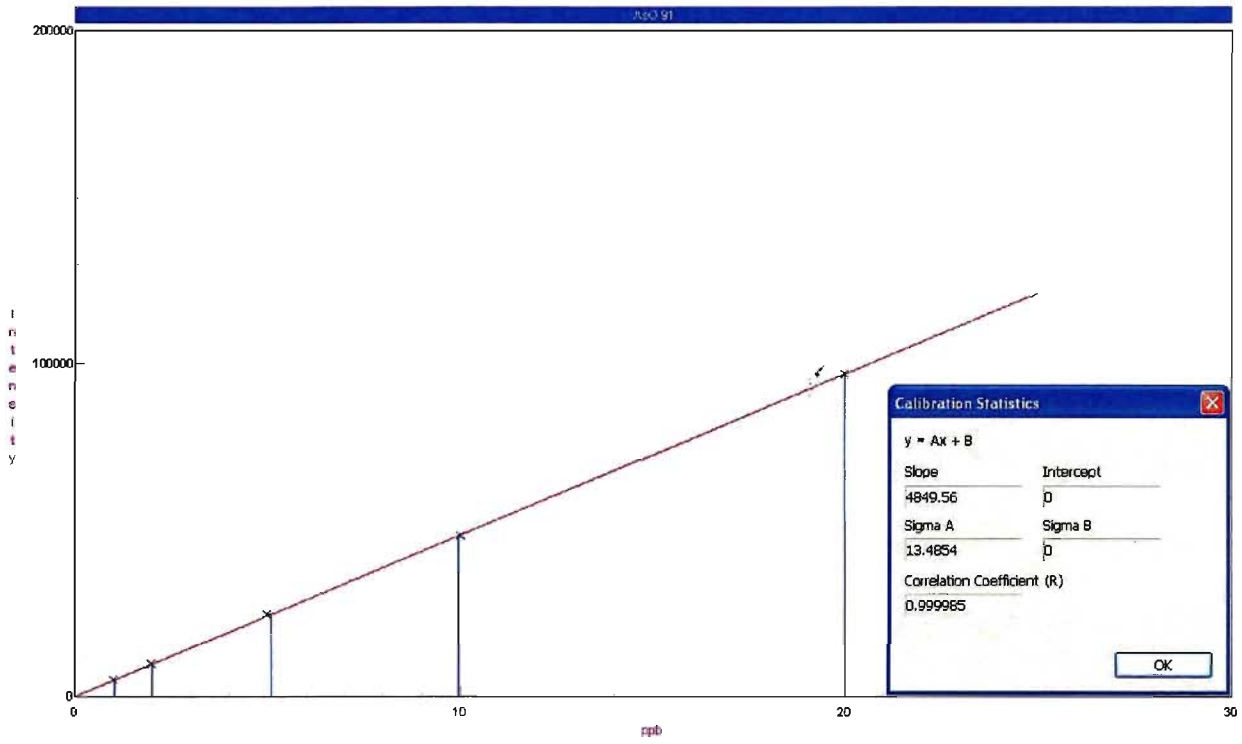

Appendix VI: continued

2. O_2 as reaction gas to produce $^{78}Se^{16}O$ (calibration range 0-100 ppb)